Physica A 483 (2017) 438–455

Contents lists available at ScienceDirect

Physica A

journal homepage: www.elsevier.com/locate/physa

Weibull thermodynamics: Subexponential decay in the energy spectrum of cosmic-ray nuclei

Roman Tomaschitz

Sechsschimmelgasse 1/21-22, A-1090 Vienna, Austria

HIGHLIGHTS

- A spectral fit to the ultra-high energy flux of cosmic-ray nuclei exhibits subexponential Weibull decay.
- The spectral number density of the nuclear gas is a multiply broken power-law distribution with Weibull cutoff.
- The thermodynamics of a stationary non-equilibrium gas of relativistic nuclei is developed, starting with the entropy functional in phase space.
- The heat capacities, compressibilities and the expansion coefficient of a relativistic gas mixture in stationary non-equilibrium are derived.
- Estimates of temperature, number count, internal energy and pressure of the all-particle cosmic-ray flux.

ARTICLE INFO

Article history:
Received 28 October 2016
Received in revised form 10 February 2017
Available online 4 April 2017

Keywords:
Subexponential spectral decay
Entropy of stationary non-equilibrium ensembles
Weibull entropy and excess entropy
Multiply broken power-law densities with Weibull cutoff
Heat capacities of a non-equilibrated gas mixture
Thermodynamics of cosmic-ray nuclei

ABSTRACT

The spectral number density of cosmic-ray nuclei is shown to be a multiply broken power law with subexponential spectral cutoff. To this end, a spectral fit is performed to data sets covering the $1\,\text{GeV}-10^{11}$ GeV interval of the all-particle cosmic-ray spectrum. The flux points of the ultra-high energy spectral tail measured with the Telescope Array indicate a Weibull cutoff $\exp(-(E/(k_BT))^\sigma)$ and permit a precise determination of the cutoff temperature $k_BT = (2.5 \pm 0.1) \times 10^{10}$ GeV and the spectral index $\sigma = 0.66 \pm 0.02$. Based on the spectral number density inferred from the least-squares fit, the thermodynamics of this stationary non-equilibrium system, a multi-component mixture of relativistic nuclei, is developed. The derivative of entropy with respect to internal energy defines the effective temperature of the nuclei, $S_{,U} = 1/T_{\text{eff}}$, $k_BT_{\text{eff}} \approx 16.1$ GeV, and the functional dependence between the cutoff temperature in the Weibull exponential and the effective gas temperature is determined. The equipartition ratio is found to be $U/(Nk_BT_{\text{eff}}) \approx 0.30$. The isochoric and isobaric heat capacities of the nuclear gas are calculated, as well as the isothermal and adiabatic compressibilities and the isobaric expansion coefficient, and it is shown that this non-equilibrated relativistic gas mixture satisfies the thermodynamic inequalities $0 < C_V < C_P$ and $0 < \kappa_S < \kappa_{T_{\text{eff}}}$.

© 2017 Elsevier B.V. All rights reserved.

1. Introduction

We discuss the thermodynamics of the all-particle cosmic-ray spectrum which has recently been measured over an extended energy range by several ground-based, balloon- and space-borne experiments [1–9]. The spectrum comprises relativistic nuclei with energies ranging from 1 GeV to 10^{11} GeV, and the measurements are sufficiently precise to reveal the

E-mail address: tom@geminga.org.

http://dx.doi.org/10.1016/j.physa.2017.03.034
0378-4371/© 2017 Elsevier B.V. All rights reserved.

spectral fine structure. In double-logarithmic representation, the wideband spectral map consists of multiple power-law slopes with smooth transitions at the spectral breaks, terminating with a subexponential spectral cutoff above 10^{10} GeV.

The purpose of this paper is to model the spectral fine structure. *Ab initio* modeling of the cosmic ray flux based on kinetic equations requires to quantify the driving forces sustaining the stationary non-equilibrium, that is the production sites and acceleration and attenuation mechanisms as well as the nuclear mass composition, which are only vaguely known [10,11]. Numerical simulations suggest that protons can be accelerated up to a few 10^6 GeV by diffusive shock acceleration in supernova remnants, and iron nuclei up to 10^8 GeV. Direct evidence for that is still lacking, as there are no intensity peaks in anisotropy maps which can be associated with specific remnants. Another Galactic driving mechanism is acceleration in the electric fields of pulsars. Ultra-high energy cosmic rays above 10^8 GeV are believed to be of extragalactic origin. If these rays are predominantly protons, the spectral cutoff could stem from energy dissipation due to scattering by background photons. Another possible attenuation effect at ultra-high energies is photo-disintegration of heavier nuclei. The cutoff could also be caused by acceleration limits at the production sites. As ab initio modeling of the wideband fine structure is presently not a viable option owing to the uncertain production and interaction mechanisms, we will content ourselves with a reconstruction of the spectral density from the available data sets. We will treat cosmic-ray nuclei as a relativistic gas in stationary non-equilibrium, as the cosmic-ray flux does not change on accessible time scales, apart from solar modulations at low energy which are already averaged out in the data sets. We will also dissect the entropy functional of the empirical spectral density to characterize the deviation from equilibrium, which can be done quantitatively without specification of the driving forces as outlined below.

The spectral flux density extending over eleven decades in energy can be fitted by a multiply broken power-law distribution with a subexponential spectral cutoff at ultra-high energies. The measured subexponential spectral decay means to replace the Boltzmann factor in the flux density by the Weibull factor $\exp(-(E/(k_BT))^\sigma)$ with spectral index (shape parameter) $0 < \sigma < 1$ [12,13], also known as stretched exponential or Kohlrausch function in relaxation theory [14,15]. In Sections 2 and 3, we develop the thermodynamic formalism of a classical stationary non-equilibrium system described by a power-law density admitting subexponential Weibull decay. In Sections 4 and 5, we employ power-law densities with Weibull cutoff to perform a spectral fit to the all-particle cosmic-ray spectrum and to estimate the thermodynamic parameters of this relativistic nuclear gas.

Cosmic-ray nuclei can be treated as a classical gas, quantum corrections as well as the Coulomb interaction being negligible due to their low fugacity and density and high temperature. Relativistic statistical systems with short- and long-range interactions exhibiting quantum effects are studied in Refs. [16–20] and references therein, pertaining to conceptual topics like negative heat capacities [16] and negative entropy [17] as well as to concrete applications such as astrophysical electron plasmas [18–20]. Astro- and geophysical applications of sub- and superexponential Weibull factors (stretched and compressed exponentials with shape parameters $\sigma < 1$ and $\sigma > 1$, respectively) include asteroid fragmentation statistics [21], speed distributions of planetary surface winds [22–24] and earthquake interevent times [25–27]. Examples of network applications of the Weibull distribution can be found in Refs. [28–31], ranging from traffic flows to market volatility. The original use of the Weibull distribution as empirical fracture probability of brittle solids is discussed in Refs. [32,33]. A deformation of the Weibull density interpolating between the stretched exponential distribution and Pareto power laws [34] was used in Ref. [35] to model income distributions. Applications thereof in reliability modeling and weakest link theory are discussed in Refs. [36,37]. Multi-parameter exponential densities with Pareto tails were also employed in Ref. [38] to model wealth distributions etc.

In the following, we give an outline of this paper. In Section 2, we study the entropy of a stationary non-equilibrium gas (classical, relativistic) defined by a spectral number density composed of a multiply broken power law and a Weibull exponential. Comparing with the entropy function of an equilibrium system, there are two major differences. The contribution U/T of the internal energy to the entropy functional is replaced by the Weibull entropy accounting for the subexponential spectral decay, and the power-law factor in the number density describing the spectral breaks gives rise to an additional term in the entropy functional, the excess entropy which vanishes in an equilibrium system. Integral representations of Weibull and excess entropy suitable for numerical evaluation are also provided in Section 2. We also sketch the derivation of the spectral number density from the probability distribution in phase space, and derive excess entropy, Weibull entropy and total entropy as phase-space expectation values, the latter in $-k_BP\log P$ representation where P is the phase-space probability. We also briefly consider phase-space fluctuations of a stationary non-equilibrium gas, and show how to express the variances, covariances and higher-order correlations of the various thermodynamic variables by derivatives of the partition function. Like in an equilibrium system, the relative fluctuations vanish in the thermodynamic limit.

In Section 3, we make use of the entropy variable to define the effective temperature of a stationary non-equilibrium gas. As the Boltzmann factor is replaced by the Weibull exponential and also because of the power-law factor in the spectral number density, the cutoff temperature k_BT in the Weibull exponential differs from the effective gas temperature defined as the reciprocal energy derivative of entropy, $T_{\rm eff} = 1/S_{,U}$. The effective chemical potential is obtained in like manner as entropy derivative with respect to the number count, $\mu_{\rm eff} = -S_{,N}/\beta_{\rm eff}$. We also find the explicit relation $\beta_{\rm eff}(\beta)$ between the effective temperature and the cutoff temperature in the Weibull factor, in terms of the temperature parameters $\beta_{\rm eff} = 1/(k_BT_{\rm eff})$ and $\beta = 1/(k_BT)^\sigma$, where σ is the Weibull spectral index. Another basic difference compared to an equilibrium system is the pressure variable, which is unrelated to the partition function (unlike in equilibrium, where $\beta PV = \log Z$ holds) and has to be assembled from the spectral number density, the particle momentum and the particle speed. We relate the pressure variable to the effective temperature, to obtain the thermal equation of state, and also derive

the caloric equation relating the internal energy to $T_{\rm eff}$. The isochoric and isobaric heat capacities are derived from the entropy variable, and we show that the inequalities $0 < C_V < C_P$ are equivalent to a positive effective temperature parameter with positive derivative $\beta'_{\rm eff}(\beta)$. Subject to the same conditions, the isobaric expansion coefficient is positive, and the isothermal and adiabatic compressibilities satisfy $0 < \kappa_S < \kappa_{T_{\rm eff}}$. To summarize Section 3, we study the entropy function of a stationary non-equilibrium gas in various parametrizations, derive numerically tame integral representations of the thermodynamic variables, and discuss positivity properties and thermodynamic inequalities relating to subexponential spectral decay.

In Section 4, we perform spectral fits to the all-particle cosmic-ray spectrum, employing the spectral densities discussed in Sections 2 and 3. The nuclei constituting the all-particle flux can roughly be divided into a light component of protons and helium, an intermediate-mass component of nitrogen-like nuclei, and a heavy iron-like component. In the $1\,\text{GeV}-10^4$ GeV range, the spectrum consists almost entirely, up to a fraction of one percent, of protons and helium nuclei. The proton and helium fluxes in this energy range have been measured by the Alpha Magnetic Spectrometer (AMS-02) on the International Space Station [1,2] and by the balloon-borne CREAM experiment [3]. In the $10^5\,\text{GeV}-10^{11}$ GeV interval, the mass composition is not yet known, although there exist some preliminary qualitative studies [6,9]. This is the ultra-relativistic regime, where the nuclear mass becomes negligible compared to the particle energy. The all-particle spectrum, irrespectively of the nuclear mass composition, has been measured in this energy range by several ground-based experiments employing Cherenkov counters and fluorescence and scintillator detectors, such as Tibet-III [4], IceTop-73 [5,6], KASCADE-Grande [7], Auger [8] and Telescope Array [9].

We first perform spectral fits to the AMS-02 proton and helium spectra in the $1\,\text{GeV}–10^4$ GeV interval. The all-particle spectrum in this interval can be approximated by adding the proton and helium fluxes. We then analytically extend the low-energy proton and helium fluxes into the $10^5\,\text{GeV}-10^{11}$ GeV interval and perform a separate fit to the all-particle spectrum in this energy range. At energies above 10^4 GeV, heavier nuclei can be accommodated in the extended proton and helium components, as the nuclear mass drops out of the flux density in this ultra-relativistic regime. The nuclear gas can thus be treated as a two-component mixture: In the $1\,\text{GeV}-10^4$ GeV interval, the flux density depends on the proton and helium (alpha particle) mass, and it becomes mass independent in the $10^4\,\text{GeV}-10^{11}$ GeV interval. The all-particle flux can therefore be represented, over the complete $1\,\text{GeV}-10^{11}$ GeV spectral range, as the sum of two partial fluxes (one depending on the proton mass and one on the helium mass), which are defined by multiply broken power-law densities with the same subexponential spectral cutoff $\exp(-(E/(k_{\rm B}T))^\sigma)$. The cutoff temperature inferred from the spectral fit is $k_{\rm B}T = (2.5 \pm 0.1) \times 10^{10}$ GeV, and the Weibull index is $\sigma = 0.66 \pm 0.02$, so that the spectral decay substantially deviates from an exponential Boltzmann cutoff.

To obtain the thermodynamic parameters of the all-particle cosmic-ray spectrum, we need to generalize the formalism developed in Section 3 to cover a multi-component gas mixture, owing to the different particle masses. It suffices to consider a two-component mixture, as the flux density only depends on the hydrogen and helium mass at low energy and is mass independent in the ultra-relativistic regime. The thermodynamics of a two-component mixture in stationary non-equilibrium is elaborated in Section 5. First, we extract the spectral number densities of the gas components from the two partial fluxes constituting the all-particle flux. Then we assemble the entropy variable of this non-equilibrated mixture and calculate the effective gas temperature, $k_{\rm B}T_{\rm eff} \approx 16$ GeV, from the energy derivative of entropy. In an equilibrium system, this temperature would coincide with the cutoff temperature in the Boltzmann factor. Because of the multiply broken power-law function in the spectral densities and the subexponential spectral decay, the cutoff temperature $k_{\rm B}T \approx 2.5 \times 10^{10}$ GeV in the Weibull factor greatly differs from the actual gas temperature $T_{\rm eff}$. We also determine the effective chemical potentials of the gas components, derive the thermal and caloric equations of state, and give estimates of the internal energy and pressure of cosmic-ray nuclei. As done in Section 3 for a one-component gas, we calculate the heat capacities and compressibilities of a two-component mixture in stationary non-equilibrium, and verify the inequalities $0 < C_V < C_P$ and $0 < \kappa_S < \kappa_{T_{\rm eff}}$ as well as the positivity of the expansion coefficient of the nuclear gas. In Section 6, we present our conclusions.

2. Entropy of a classical relativistic gas in stationary non-equilibrium

2.1. Subexponential spectral decay

We will study a relativistic gas in stationary non-equilibrium defined by the spectral number density [39,40]

$$\mathrm{d}\rho(p) = \frac{4\pi s}{(2\pi\hbar c)^3}\exp[-\alpha-\beta(p^2+m^2)^{\sigma/2}]h(p)p^2\mathrm{d}p, \tag{2.1}$$

where p is the momentum variable of the particles, $\sigma > 0$ the Weibull spectral index, $\beta = 1/(k_{\rm B}T)^\sigma$ the temperature parameter, m the particle mass, s the spin degeneracy and $f = \mathrm{e}^{-\alpha}$ the fugacity. The dimensionless spectral kernel $h(p)$ is a positive, multiply broken power-law function normalized as $h(0) = 1$. This kernel will be specified in Section 4, where we perform a spectral fit to a gas mixture of cosmic-ray nuclei admitting a power-law spectrum with subexponential spectral cutoff. This cutoff in (2.1) is due to the Weibull exponential $\exp(-\beta(p^2+m^2)^{\sigma/2})$; subexponential decay occurs for spectral indices $0 < \sigma < 1$. The dispersion relation of the relativistic gas particles is $E = \sqrt{p^2+m^2}$. The Weibull exponential $\exp(-\beta E^\sigma)$ coincides with the Boltzmann factor at $\sigma = 1$; the relativistic Maxwell equilibrium density is recovered by putting $h(p) = \sigma = 1$. The spectral function converges to one for small momenta, $h(p \to 0) = 1$. By approximating $p \sim m\upsilon$ in the non-relativistic limit, we can write the exponent in (2.1) as $-\hat{\alpha} - \hat{\beta}m\upsilon^2/2$, with the fugacity and temperature

parameters $\hat\alpha = \alpha + \beta m^\sigma$ and $\hat\beta = \beta\sigma m^{\sigma-1}$, so that the non-relativistic Maxwell velocity distribution is recovered. For the most part of this paper, we will put $\hbar = c = k_B = 1$. When discussing the nuclear gas in Sections 4 and 5, we will use the units p [GeV/c], $\hbar$ [GeV s] and c [m/s], so that $\mathrm{d}\rho(p)$ [m^{-3}]. Subexponential decay of the gamma-ray spectra of pulsars and supernova remnants is discussed in Refs. [41–43].

2.2. Weibull and excess entropies

To obtain integral representations of the thermodynamic variables, we employ a more general distribution function than stated in (2.1),

$$\mathrm{d}\rho(p) = \frac{4\pi s}{(2\pi)^3}\exp[-\alpha-\beta(p^2+m^2)^{\sigma/2} - \gamma\log\frac{1}{h(p)} - \delta\frac{1}{3}\frac{p^2}{\sqrt{p^2+m^2}} - \varepsilon\sqrt{p^2+m^2}]p^2\mathrm{d}p, \tag{2.2}$$

which defines the partition function $\log Z = V\int_0^\infty \mathrm{d}\rho(p)$. The densities (2.1) and (2.2) coincide at $\gamma = 1, \delta = \varepsilon = 0$, and derivatives will be taken at these values, so that the number count, internal energy and pressure read

$$N = -(\log Z)_{,\alpha} = V\int_0^\infty \mathrm{d}\rho(p) = \log Z, \tag{2.3}$$

$$U = -(\log Z)_{,\varepsilon} = V\int_0^\infty \sqrt{p^2+m^2}\,\mathrm{d}\rho(p), \tag{2.4}$$

$$PV = -(\log Z)_{,\delta} = \frac{1}{3}V\int_0^\infty \frac{p^2}{\sqrt{p^2+m^2}}\mathrm{d}\rho(p). \tag{2.5}$$

In equilibrium, where $h(p) = \sigma = 1$, the pressure is related to the partition function by $\beta PV = \log Z$, via partial integration of (2.5). The entropy variable is assembled as

$$S = \log Z - \alpha(\log Z)_{,\alpha} - \beta(\log Z)_{,\beta} - (\log Z)_{,\gamma}, \tag{2.6}$$

taken at $\gamma = 1, \delta = \varepsilon = 0$. The third term in (2.6) defines the Weibull entropy,

$$\frac{W}{\beta} = -(\log Z)_{,\beta} = V\int_0^\infty (p^2+m^2)^{\sigma/2}\mathrm{d}\rho(p), \tag{2.7}$$

so that $W = \beta U$ at $\sigma = 1$. The fourth term in (2.6) is the excess entropy

$$H = -(\log Z)_{,\gamma} = V\int_0^\infty \log\frac{1}{h(p)}\mathrm{d}\rho(p), \tag{2.8}$$

which vanishes if $h(p) = 1$. The total entropy thus reads, cf. (2.6),

$$S = (1+\alpha)N + W + H. \tag{2.9}$$

Weibull entropy and excess entropy define the deviation of S from an equilibrium entropy $S_{\mathrm{eq}} = (1+\alpha)N + \beta U$. The Weibull entropy is positive, but the excess entropy (2.8) can have either sign, since $\log(1/h(p))$ can undergo sign changes. As for the power-law spectral kernel of the nuclear gas studied in Section 4, $\log(1/h(p))$ is positive and monotonically increasing, so that H is positive as well.

2.3. Weibull probability distribution in phase space

We start with the n-particle phase-space measure

$$\mathrm{d}^{3n}(p,q) = \frac{1}{(2\pi)^{3n}}\mathrm{d}^3p_1\mathrm{d}^3q_1\mathrm{d}^3p_2\mathrm{d}^3q_2\cdots\mathrm{d}^3p_n\mathrm{d}^3q_n, \tag{2.10}$$

where the spatial d^3q_k integrations range over a volume V and the d^3p_k integrations over momentum space. The n-particle probability density leading to the spectral number density (2.2) reads

$$P_n(p) = \frac{b_n(p)}{Z}, \quad b_n(p) = \exp(-\alpha n - \beta w_n - \gamma h_n - \delta v_n - \varepsilon u_n), \tag{2.11}$$

with the random variables n and

$$w_n = \sum_{k=1}^n (p^2+m^2)^{\sigma/2}, \quad h_n = \sum_{k=1}^n \log\frac{1}{h(p_k)}, \quad v_n = \frac{1}{3}\sum_{k=1}^n \frac{p_k^2}{\sqrt{p_k^2+m^2}}, \quad u_n = \sum_{k=1}^n \sqrt{p_k^2+m^2}. \tag{2.12}$$

The normalization constant Z in (2.11) is defined by

$$\sum_{n=0}^{\infty}\frac{s^n}{n!}\int P_n(p)\mathrm{d}^{3n}(p,q)=1,\quad Z=\sum_{n=0}^{\infty}\frac{s^n}{n!}\int b_n(p)\mathrm{d}^{3n}(p,q), \tag{2.13}$$

where the summation is over the particle number n. The factorial accounts for indistinguishability, and s is the spin degeneracy. Z is the grand partition function which reads in spectral representation $\log Z = V\int_0^\infty \mathrm{d}\rho(p)$, cf. (2.3), since the integrals in (2.13) factorize.

2.4. Excess entropy, Weibull entropy and total entropy as phase-space expectation values

Differentiation of $\log Z$ in (2.13) with respect to the parameters of the exponential $b_n(p)$ in (2.11) leads to representations of the various thermodynamic variables as phase-space averages. For instance, the Weibull entropy (2.7) is assembled in phase space as

$$\frac{W}{\beta}=-(\log Z)_{,\beta}=\sum_{n=0}^{\infty}\frac{s^n}{n!}\int w_nP_n(p)\mathrm{d}^{3n}(p,q)=\langle w_n\rangle, \tag{2.14}$$

with w_n defined in (2.12). The expectation values of excess entropy $H=\langle h_n\rangle$, internal energy $U=\langle u_n\rangle$, pressure $PV=\langle v_n\rangle$ and particle number $N=\langle n\rangle$ are defined in like manner, all being taken at $\gamma=1,\delta=\varepsilon=0$. Evaluating the factorizing integrals, we arrive at the spectral representations stated in (2.3)–(2.8). The entropy variable reads

$$S=-\sum_{n=0}^{\infty}\frac{s^n}{n!}\int P_n(p)\log P_n(p)\mathrm{d}^{3n}(p,q), \tag{2.15}$$

with random variable

$$s_n=-\log P_n(p)=\log Z+\alpha n+\beta w_n+h_n, \tag{2.16}$$

so that $S=\langle s_n\rangle=\log Z+\alpha N+W+H$ as stated in (2.9). The quantized Fermionic counterparts of these phase-space averages, applicable in the nearly degenerate low-temperature regime, have been discussed in Refs. [40,44].

In contrast to an equilibrium system, the probability distribution $P_n(p)$ in (2.11) (taken at $\gamma=1,\delta=\varepsilon=0$) does not maximize the entropy functional (2.15) subject to the particle number and internal energy constraints $N=\langle n\rangle$ and $U=\langle u_n\rangle$, see after (2.14). Only the equilibrium distribution defined by $h(p)=1$ and $\sigma=1$ in (2.1) maximizes the entropy functional (2.15). To see this, we consider the equilibrium distribution $P_n^{\mathrm{eq}}(p)=b_n^{\mathrm{eq}}(p)/Z_{\mathrm{eq}}$, $b_n^{\mathrm{eq}}(p)=\exp(-\alpha_{\mathrm{eq}}n-\beta_{\mathrm{eq}}u_n)$, where Z_{eq} is defined as in (2.13) (with b_n replaced by b_n^{eq}), so that P_n^{eq} is normalized to one. The constraints prescribing $N=\langle n\rangle$ and $U=\langle u_n\rangle$ are defined as in (2.14) with P_n replaced by P_n^{eq}; the equilibrium entropy S_{eq} is defined as in (2.15), also with this replacement $P_n\to P_n^{\mathrm{eq}}$. As P_n and P_n^{eq} satisfy the same constraints, namely $N=\langle n\rangle$, $U=\langle u_n\rangle$ and the normalization (2.13), we can also average the equilibrium entropy S_{eq} over P_n instead of P_n^{eq}. That is, S_{eq} can be defined by replacing $P_n\log P_n$ in (2.15) by $P_n\log P_n^{\mathrm{eq}}$ instead of $P_n^{\mathrm{eq}}\log P_n^{\mathrm{eq}}$. Finally we consider the difference $S-S_{\mathrm{eq}}$, with S in (2.15) and S_{eq} defined by $P_n\log P_n^{\mathrm{eq}}$, and apply the general logarithmic inequality $\log(P_n/P_n^{\mathrm{eq}})>1-P_n^{\mathrm{eq}}/P_n$ and the normalization (2.13) (valid for P_n as well as P_n^{eq}) to find $S<S_{\mathrm{eq}}$.

2.5. Variances, covariances and higher-order correlations: fluctuations in stationary non-equilibrium ensembles

We calculate the variances of the particle number $\langle(\Delta n)^2\rangle$, Weibull entropy $\langle(\Delta w_n)^2\rangle$, excess entropy $\langle(\Delta h_n)^2\rangle$, pressure $\langle(\Delta v_n)^2\rangle$ and internal energy $\langle(\Delta u_n)^2\rangle$, using the phase-space random variables in (2.12) and the shortcuts $\Delta n=n-\langle n\rangle$, $\Delta w_n=w_n-\langle w_n\rangle$, etc. The variances $\langle(\Delta n)^2\rangle=\langle n^2\rangle-\langle n\rangle^2$, $\langle(\Delta w_n)^2\rangle=\langle w_n^2\rangle-\langle w_n\rangle^2$, etc., are then obtained as second derivatives of $\log Z$. For instance, $\langle(\Delta n)^2\rangle=(\log Z)_{,\alpha,\alpha}$ and $\langle(\Delta w_n)^2\rangle=(\log Z)_{,\beta,\beta}$, taken at $\gamma=1,\delta=\varepsilon=0$. We note the pairs $(\Delta n,\alpha)$, $(\Delta w_n,\beta)$, $(\Delta h_n,\gamma)$, $(\Delta v_n,\delta)$ and $(\Delta u_n,\varepsilon)$, cf. (2.11), so that the variances and covariances like $\langle\Delta n\Delta w_n\rangle=(\log Z)_{,\alpha,\beta}$ and $\langle\Delta w_n\Delta h_n\rangle=(\log Z)_{,\beta,\gamma}$ are obtained by differentiation with the respective parameters. Higher-order correlations are assembled analogously, e.g. the triple correlations $\langle\Delta n(\Delta w_n)^2\rangle=-(\log Z)_{,\alpha,\beta,\beta}$ and $\langle\Delta u_n\Delta w_n\Delta h_n\rangle=-(\log Z)_{,\varepsilon,\beta,\gamma}$; the minus sign arises in case of an odd number of factors. Spectral representations of correlations suitable for numerical computation are thus obtained by multiple differentiation of the partition function $\log Z=V\int_0^\infty\mathrm{d}\rho(p)$ as in (2.3)–(2.8). The heat capacities and compressibilities of a gas in stationary non-equilibrium can be expressed by the expectation values in Section 2.4, their variances, covariances and triple correlations, see the remarks after (3.28).

The entropy variance $\langle(\Delta s_n)^2\rangle=\langle s_n^2\rangle-\langle s_n\rangle^2$, with $\Delta s_n=s_n-\langle s_n\rangle$, is a linear combination of the above variances and covariances, since $\Delta s_n=\alpha\Delta n+\beta\Delta w_n+\Delta h_n$, cf. (2.16). We square this to find

$$\langle(\Delta s_n)^2\rangle=\alpha^2(\log Z)_{,\alpha,\alpha}+\beta^2(\log Z)_{,\beta,\beta}+(\log Z)_{,\gamma,\gamma}+2\alpha\beta(\log Z)_{,\alpha,\beta}+2\alpha(\log Z)_{,\alpha,\gamma}+2\beta(\log Z)_{,\beta,\gamma}, \tag{2.17}$$

taken at $\gamma=1,\delta=\varepsilon=0$. The right-hand side is positive despite of the possibly negative covariances $(\log Z)_{,\alpha,\gamma}$ and $(\log Z)_{,\beta,\gamma}$, cf. after (2.9), as it is the expectation value of a square. The relative fluctuations vanish in the limit $V\to\infty$, $\sqrt{\langle(\Delta s_n)^2\rangle}/\langle s_n\rangle\propto 1/\sqrt{V}$, and the same holds for the random variables (2.12) of number count, Weibull and excess entropy, pressure and internal energy.

3. Effective temperature and Weibull spectral decay: Thermodynamics of a stationary non-equilibrium gas

3.1. (α, β, V) parametrization of thermodynamic variables

We define the partition factor z by a rescaling of $\log Z$ in (2.3) with the volume factor and the fugacity $f = \mathrm{e}^{-\alpha}$,

$$z(\beta,\gamma,\delta,\varepsilon) = \frac{\log Z}{Vf} = \int_0^\infty \mathrm{d}\hat{\rho}(p),$$

$$\mathrm{d}\hat{\rho}(p) = \frac{4\pi s}{(2\pi)^3}\exp[-\beta(p^2+m^2)^{\sigma/2} - \gamma\log\frac{1}{h(p)} - \delta\frac{1}{3}\frac{p^2}{\sqrt{p^2+m^2}} - \varepsilon\sqrt{p^2+m^2}]p^2\mathrm{d}p, \tag{3.1}$$

taken at $\gamma = 1, \delta = \varepsilon = 0$, so that z and its derivatives (denoted by a subscript comma, e.g., $z_{,\beta}, z_{,\beta,\gamma}$) only depend on the Weibull exponent $\beta = 1/(k_{\mathrm{B}}T)^\sigma$. As in Section 2.5, we consider the pairs $((p^2+m^2)^{\sigma/2}, \beta)$, $(\log(1/h(p)), \gamma)$, $(p^2/(3\sqrt{p^2+m^2}), \delta)$ and $(\sqrt{p^2+m^2}, \varepsilon)$. Multiple differentiation of $z(\beta,\gamma,\delta,\varepsilon)$ with respect to the indicated parameters generates the respective p dependent factors in the integrand of (3.1), as well as a minus sign if there is an odd number of derivatives. In this way, we arrive at numerically tame integral representations of $z(\beta,\gamma,\delta,\varepsilon)$ and its derivatives.

All thermodynamic variables can efficiently be expressed and calculated in terms of the partition factor and its derivatives. Particle number, internal energy and pressure read, cf. (2.3)–(2.5),

$$N = V\mathrm{e}^{-\alpha}z, \quad U = -V\mathrm{e}^{-\alpha}z_{,\varepsilon}, \quad P = -\mathrm{e}^{-\alpha}z_{,\delta}. \tag{3.2}$$

Weibull entropy, excess entropy and total entropy are assembled as, cf. (2.6)–(2.9),

$$W/\beta = -V\mathrm{e}^{-\alpha}z_{,\beta}, \quad H = -V\mathrm{e}^{-\alpha}z_{,\gamma}, \tag{3.3}$$

$$S(\alpha,\beta,V) = V\mathrm{e}^{-\alpha}((1+\alpha)z - \beta z_{,\beta} - z_{,\gamma}). \tag{3.4}$$

The (α, β, V) representation is convenient when calculating thermodynamic variables from an empirical flux density obtained by a spectral fit, see Section 5. Other variables such as the effective temperature and the heat capacities of a stationary non-equilibrium gas will be derived in different representations but will ultimately be calculated in (α, β, V) parametrization.

3.2. (β, V, N) parametrization of internal energy, pressure and entropy

We invert the first identity in (3.2), $\alpha = \log(zV/N)$, to find the (β, V, N) representation of internal energy and pressure as

$$U(\beta,N) = Nu(\beta), \quad u(\beta) = -\frac{z_{,\varepsilon}}{z}, \tag{3.5}$$

$$P = \eta(\beta)\frac{N}{V}, \quad \eta(\beta) = -\frac{z_{,\delta}}{z}, \tag{3.6}$$

and the entropy variable

$$S(\beta,V,N) = N\left(1 - \log\frac{N}{V} + s(\beta)\right), \quad s(\beta) = \log z - \beta\frac{z_{,\beta}}{z} - \frac{z_{,\gamma}}{z}. \tag{3.7}$$

3.3. Entropy in (U, V, N) parametrization: effective temperature and effective chemical potential

To eliminate the temperature variable β in the (β, V, N) representation, we invert $U = Nu(\beta)$ in (3.5), $\beta = u^{-1}(U/N)$, to find, cf. (3.7),

$$S(U,V,N) = N[1 - \log(N/V) + s(u^{-1}(U/N))]. \tag{3.8}$$

The effective temperature parameter $\beta_{\mathrm{eff}} = 1/(k_{\mathrm{B}}T_{\mathrm{eff}})$ and the effective fugacity parameter α_{eff} are defined by the entropy derivatives

$$S_{,U} = \beta_{\mathrm{eff}}, \quad \beta_{\mathrm{eff}}(\beta) = \frac{s'(\beta)}{u'(\beta)}, \tag{3.9}$$

$$S_{,N} = \alpha_{\mathrm{eff}}, \quad \alpha_{\mathrm{eff}} = -\log\frac{N}{V} + s(\beta) - \frac{U}{N}\frac{s'(\beta)}{u'(\beta)}, \tag{3.10}$$

where, cf. (3.5) and (3.7),

$$u'(\beta) = -z^{-2}(zz_{,\varepsilon,\beta} - z_{,\varepsilon}z_{,\beta}), \quad s'(\beta) = -z^{-2}[\beta(zz_{,\beta,\beta} - z_{,\beta}z_{,\beta}) + (zz_{,\gamma,\beta} - z_{,\gamma}z_{,\beta})]. \tag{3.11}$$

The effective fugacity is $f_{\rm eff} = {\rm e}^{-\alpha_{\rm eff}}$ and the effective chemical potential $\mu_{\rm eff} = -\alpha_{\rm eff}/\beta_{\rm eff}$ reads

$$\mu_{\rm eff} = \frac{1}{\beta_{\rm eff}} \log \frac{N}{V} + u(\beta) - \frac{s(\beta)}{\beta_{\rm eff}}. \tag{3.12}$$

We also note $S_{,V} = N/V = P/\eta(\beta)$, according to (3.6) and (3.8). In equilibrium (where $h(p) = 1$ and $\sigma = 1$ in spectral densities (2.1) and (2.2)), we find $\beta_{\rm eff} = \beta$, $\alpha_{\rm eff} = \alpha$ and the thermal scale factor $\eta(\beta) = 1/\beta$ in (3.6), the latter by partial integration of the partition factor (3.1). In contrast to an equilibrium gas, where temperature and chemical potential are parameters in the spectral number density, the effective temperature and effective chemical potential of a stationary non-equilibrium system are globally defined by the partition factor z and its derivatives, which are averages over the number density, cf. (3.1). Positivity properties of the functions $u(\beta)$, $\eta(\beta)$, $s(\beta)$, $\beta_{\rm eff}(\beta)$ and their derivatives will be discussed in Section 3.8.

In Section 5, we will obtain the effective temperature and the chemical potential from a spectral fit. Conceptually, it is also possible to infer these parameters by equilibration with a thermal system. For notational simplicity, we assume this reference system to be a free relativistic gas defined by number density (2.1) with $h(p) = 1$ and $\sigma = 1$. The entropy function and the variables of this thermometer system are labeled with a subscript of two: $S_2(U_2, V_2, N_2)$, so that $S_{2,U_2} = \beta_2$, $S_{2,V_2} = \beta_2 P_2$ and $S_{2,N_2} = \alpha_2$, with chemical potential $\mu_2 = -\alpha_2/\beta_2$ and thermal equation $\beta_2 P_2 = N_2/V_2$.

We keep the particle numbers N and N_2 constant. When equilibrating $S(U, V, N)$ in (3.8) and $S_2(U_2, V_2, N_2)$, we use as contact variables $\beta_{\rm eff} = \beta_2 =: \beta_{\rm c}$ and $P = P_2$. The total energy and volume are kept constant, $U + U_2 = U_{\rm tot}$, $V + V_2 = V_{\rm tot}$. We thus find the equations $S_{2,U}(U, V, N) = \beta_{\rm c}$ and $S_{2,U_2}(U_2, V_2, N_2) = \beta_{\rm c}$, and the pressure identity gives $\eta(\beta(\beta_{\rm c}))N/V = N_2/(\beta_{\rm c}V_2)$ by way of the thermal equations, cf. (3.6). (In the thermal scale factor $\eta(\beta)$, we have substituted $\beta = \beta(\beta_{\rm eff})$, which is the inversion of $\beta_{\rm eff}(\beta)$, cf. (3.9).) Together with the conservation conditions $U + U_2 = U_{\rm tot}$ and $V + V_2 = V_{\rm tot}$, we obtain five equations to determine the variables U, U_2, V, V_2 and $\beta_{\rm c}$; the latter is a Lagrange parameter used to maximize $S(U, V, N) + S_2(U_2, V_2, N_2)$ with respect to the energy variables subject to the constraint $U + U_2 = U_{\rm tot}$. The total entropy $S + S_2$ is not maximized with respect to the volume variables V and V_2, as this would require to equate $P/\eta(\beta(\beta_{\rm c})) = P_2\beta_{\rm c}$ instead of the pressure variables, $P = P_2$. Only if $\eta(\beta(\beta_{\rm c})) = 1/\beta_{\rm c}$, which happens if $S(U, V, N)$ is an equilibrium entropy, the contact identity $P = P_2$ amounts to maximize the total entropy $S + S_2$ also with respect to the volume variables subject to $V + V_2 = V_{\rm tot}$. This reflects the fact that the phase-space probability distribution $P_n(p)$ in (2.11) does not maximize the entropy functional (2.15); only the equilibrium distribution $P_n^{\rm eq}(p)$ gives the maximum entropy, see after (2.16). In brief, the stationary non-equilibrium entropy (3.4) is always smaller than the equilibrium entropy if subjected to the same constraints.

3.4. Entropy in $(\beta_{\rm eff}, V, N)$ parametrization, thermal and caloric equations of state, and isochoric heat capacity

We use the effective temperature parameter $\beta_{\rm eff} = s'(\beta)/u'(\beta)$ in (3.9) as independent variable, and substitute the inversion $\beta = \beta(\beta_{\rm eff})$ into the (β, V, N) representation in Section 3.2. The existence of this inversion is assured by the positivity conditions $\beta_{\rm eff}(\beta) > 0$ and $\beta'_{\rm eff}(\beta) > 0$, see Section 3.8, but we will not need to perform it explicitly. The caloric and thermal equations of state read $U = Nu(\beta(\beta_{\rm eff}))$ and $P = \eta(\beta(\beta_{\rm eff}))N/V$, cf. (3.5) and (3.6), and the $(\beta_{\rm eff}, V, N)$ representation of entropy is, cf. (3.7),

$$S(\beta_{\rm eff}, V, N) = N[1 - \log(N/V) + s(\beta(\beta_{\rm eff}))]. \tag{3.13}$$

The isochoric heat capacity $C_V = T_{\rm eff}S_{,T_{\rm eff}}(\beta_{\rm eff}, V, N)$ reads

$$C_V = -\beta_{\rm eff}S_{,\beta_{\rm eff}}(\beta_{\rm eff}, V, N) = -N\beta_{\rm eff}^2 \frac{u'(\beta)}{\beta'_{\rm eff}(\beta)}. \tag{3.14}$$

To calculate the derivative of the effective temperature $\beta'_{\rm eff}(\beta) = (s'' - u''\beta_{\rm eff})/u'$ required here, we use u' and s' in (3.11), the second derivatives

$$\begin{aligned} u''(\beta) &= z^{-3}[z(z_{,\varepsilon}z_{,\beta,\beta} - zz_{,\varepsilon,\beta,\beta}) + 2z_{,\beta}(zz_{,\varepsilon,\beta} - z_{,\varepsilon}z_{,\beta})], \\ s''(\beta) &= z^{-3}[\beta z(z_{,\beta}z_{,\beta,\beta} - zz_{,\beta,\beta,\beta}) + 2\beta_{\rm eff}z_{,\beta}(zz_{,\varepsilon,\beta} - z_{,\varepsilon}z_{,\beta}) + z(z_{,\gamma}z_{,\beta,\beta} - zz_{,\gamma,\beta,\beta}) - z(zz_{,\beta,\beta} - z_{,\beta}z_{,\beta})], \end{aligned} \tag{3.15}$$

and the integral representation (3.1) of the partition factor z and its derivatives. Finally, the Helmholtz free energy $F = U - S/\beta_{\rm eff}$ admits derivatives analogous to an equilibrium system, $F_{,\beta_{\rm eff}} = S/\beta_{\rm eff}^2$, $F_{,N} = \mu_{\rm eff}$, with the effective chemical potential $\mu_{\rm eff}$ in (3.12), and $F_{,V} = -N/(V\beta_{\rm eff})$, where we can substitute the thermal equation $N/V = P/\eta(\beta(\beta_{\rm eff}))$.

3.5. Internal energy in (S, V, N) parametrization

We invert $S(\beta, V, N)$ in (3.7), solving for β,

$$\beta = s^{-1}\left(\frac{S}{N} - 1 + \log\frac{N}{V}\right), \tag{3.16}$$

to find, cf. (3.5),

$$U(S,V,N) = Nu\left(s^{-1}\left(\frac{S}{N} - 1 + \log\frac{N}{V}\right)\right). \tag{3.17}$$

We note the derivatives $U_{,S} = 1/\beta_{\rm eff}$, $U_{,N} = \mu_{\rm eff}$, cf. (3.9) and (3.12), and $U_{,V} = -N/(V\beta_{\rm eff})$.

3.6. Entropy and volume in $(\beta_{\rm eff}, P, N)$ parametrization: isobaric heat capacity, isothermal compressibility and isobaric expansion coefficient

By way of the thermal equation in Section 3.4, the volume can be parametrized as

$$V(\beta_{\rm eff}, P, N) = \eta(\beta(\beta_{\rm eff}))\frac{N}{P}. \tag{3.18}$$

The internal energy $U = Nu(\beta(\beta_{\rm eff}))$ reads as in Section 3.4, since it is independent of the volume factor. The entropy in $(\beta_{\rm eff}, P, N)$ representation is obtained by eliminating the volume in (3.13) by substitution of (3.18),

$$S(\beta_{\rm eff}, P, N) = N[1 - \log P + g(\beta(\beta_{\rm eff}))], \quad g(\beta) = s(\beta) + \log\eta(\beta). \tag{3.19}$$

The $\beta_{\rm eff}$ derivative thereof is

$$S_{,\beta_{\rm eff}}(\beta_{\rm eff}, P, N) = N\frac{g'(\beta)}{\beta'_{\rm eff}(\beta)} = S_{,\beta_{\rm eff}}(\beta_{\rm eff}, V, N) + \frac{N}{\beta'_{\rm eff}(\beta)}\frac{\eta'(\beta)}{\eta(\beta)}, \tag{3.20}$$

with $S_{,\beta_{\rm eff}}(\beta_{\rm eff}, V, N)$ as in (3.14). The derivatives of $\eta(\beta)$ in (3.6) and $g(\beta)$ in (3.19) read, cf. (3.9) and (3.11),

$$g'(\beta) = \beta_{\rm eff}u'(\beta) + \frac{\eta'(\beta)}{\eta(\beta)}, \quad \eta'(\beta) = -\frac{zz_{,\beta,\delta} - z_{,\delta}z_{,\beta}}{z^2}. \tag{3.21}$$

The isobaric specific heat $C_P = T_{\rm eff}S_{,T_{\rm eff}}(\beta_{\rm eff}, P, N)$ can be read off from the entropy derivative in (3.20),

$$C_P = -\beta_{\rm eff}S_{,\beta_{\rm eff}}(\beta_{\rm eff}, P, N) = C_V - \frac{N\beta_{\rm eff}}{\beta'_{\rm eff}(\beta)}\frac{\eta'(\beta)}{\eta(\beta)}. \tag{3.22}$$

In Section 3.8, we will show that $C_P > C_V > 0$ follows from the positivity of $\beta_{\rm eff}(\beta)$ and $\beta'_{\rm eff}(\beta)$.

The derivatives of the volume factor $V(\beta_{\rm eff}, P, N)$ in (3.18),

$$V_{,\beta_{\rm eff}} = \frac{\eta'(\beta)}{\beta'_{\rm eff}(\beta)}\frac{N}{P}, \quad V_{,P} = -\eta(\beta)\frac{N}{P^2}, \tag{3.23}$$

define the isothermal compressibility, $\kappa_{T_{\rm eff}} = -V_{,P}/V = 1/P$, and the isobaric expansion coefficient,

$$\alpha_{\rm exp} = \frac{V_{,T_{\rm eff}}}{V} = -\beta_{\rm eff}^2\frac{V_{,\beta_{\rm eff}}}{V} = -\frac{\beta_{\rm eff}^2}{\beta'_{\rm eff}(\beta)}\frac{\eta'(\beta)}{\eta(\beta)}. \tag{3.24}$$

We also note $C_P = C_V + N\alpha_{\rm exp}/\beta_{\rm eff}$, cf. (3.22). In equilibrium, $\alpha_{\rm exp} = \beta_{\rm eff} = \beta$.

3.7. Volume in (S, P, N) parametrization: adiabatic compressibility

We start with the entropy representation in (3.19) and solve for β,

$$\beta = g^{-1}(S/N - 1 + \log P). \tag{3.25}$$

The derivative of $\beta_{\rm eff}(\beta(S,P,N))$ with respect to pressure is thus $\beta_{{\rm eff},P} = \beta'_{\rm eff}(\beta)/(Pg'(\beta))$. The volume $V(S,P,N)$ is obtained by substituting β defined by (3.25) into the thermal equation (3.6),

$$V(S,P,N) = \eta(g^{-1}(S/N - 1 + \log P))\frac{N}{P}. \tag{3.26}$$

The pressure derivative of $V(S,P,N)$ is then found as

$$V_{,P} = \left(\frac{\eta'(\beta)}{\eta(\beta)}\frac{1}{g'(\beta)} - 1\right)\eta(\beta)\frac{N}{P^2}. \tag{3.27}$$

The derivatives $\eta'(\beta)$ and $g'(\beta)$ are stated in (3.21). The adiabatic compressibility reads

$$\kappa_S = -\frac{V_{,P}}{V} = \frac{\kappa_{T_{\rm eff}}}{1 + C_R}, \quad C_R(\beta) = \frac{1}{\beta_{\rm eff}(\beta)u'(\beta)}\frac{\eta'(\beta)}{\eta(\beta)}, \tag{3.28}$$

with $\kappa_{T_{\rm eff}} = 1/P$, cf. after (3.23). The heat capacity ratio is $\gamma_R = C_P/C_V = 1 + C_R$, cf. (3.14) and (3.22), and thus $\kappa_{T_{\rm eff}}/\kappa_S = C_P/C_V$.

In the energy density $u(\beta)$ and the thermal scale factor $\eta(\beta)$ in (3.5) and (3.6), z can be replaced by $\log Z$, as the volume factor and the fugacity $f = \mathrm{e}^{-\alpha}$ in (3.1) scale out. The same holds for the derivatives of $u(\beta)$, $s(\beta)$ and $\eta(\beta)$ in (3.11), (3.15) and (3.21), so that they can be expressed by the expectation values and correlations derived in Sections 2.4 and 2.5. For instance, $\log Z = \langle n\rangle$, $(\log Z)_{,\beta} = -\langle w_n\rangle$, $(\log Z)_{,\gamma,\beta} = \langle \Delta h_n \Delta w_n\rangle$ and $(\log Z)_{,\varepsilon,\beta,\beta} = -\langle \Delta u_n(\Delta w_n)^2\rangle$. This also holds true for the effective temperature parameter $\beta_{\mathrm{eff}}(\beta)$ and its derivative, cf. (3.9) and (3.15), as well as for the heat capacities (3.14) and (3.22), the expansion coefficient (3.24) and the compressibilities in (3.28), as they are assembled from the mentioned quantities.

3.8. Positivity of heat capacity, compressibility and expansion coefficient

To discuss positivity properties, we need the Chebyshev integral inequality

$$\int_0^\infty \mathrm{d}\hat\rho(p)\int_0^\infty AB\mathrm{d}\hat\rho(p) \geq \int_0^\infty A\mathrm{d}\hat\rho(p)\int_0^\infty B\mathrm{d}\hat\rho(p), \tag{3.29}$$

where $\mathrm{d}\hat\rho(p)$ is the spectral measure in (3.1) and $A(p)$ and $B(p)$ are monotonic functions with the same monotonicity. (That is, their first derivatives are both positive or negative.) In the case of opposite monotonicity, the inequality sign is evidently reversed. If $A = B$, this holds without monotonicity requirement and becomes a special case of the Cauchy–Schwarz inequality.

The energy density $u(\beta) = -z_{,\varepsilon}/z$ defining the internal energy in (3.5) is positive, which follows from the integral representation of z and $z_{,\varepsilon}$, cf. (3.1). The derivative $u'(\beta)$ in (3.11) is negative, which follows from the Chebyshev inequality. A positive effective temperature $\beta_{\mathrm{eff}} = s'(\beta)/u'(\beta)$, cf. (3.9), is thus tantamount to a negative derivative $s'(\beta)$; the first term of $s'(\beta)$ in (3.11) is negative according to the Chebyshev inequality, but the second term can be positive and overpower the first term, since γ differentiation of z generates the factor $\log h(p)$ in the integrand of (3.1), which is in general not a monotonic function so that the Chebyshev inequality is not applicable. Positivity of the effective temperature β_{eff} as well as a positive derivative $\beta'_{\mathrm{eff}}(\beta)$ are necessary and sufficient conditions for the thermodynamic inequalities discussed below. In an equilibrium system, these conditions are always satisfied, since $\beta_{\mathrm{eff}} = \beta$.

The thermal scale factor $\eta(\beta) = -z_{,\delta}/z$ in (3.6) is positive, which follows from the integral representation of z and $z_{,\delta}$, cf. (3.1). Its derivative, $\eta'(\beta)$ in (3.21) is negative according to the Chebyshev inequality. The heat capacities thus satisfy $C_P > C_V > 0$, cf. (3.14) and (3.22), if $\beta_{\mathrm{eff}} > 0$ and $\beta'_{\mathrm{eff}}(\beta) > 0$. As for the compressibilities, the coefficient $C_R(\beta)$ in (3.28) defining the compressibility ratio is positive if $\beta_{\mathrm{eff}} > 0$ (since $\eta'(\beta) < 0$, $u'(\beta) < 0$ and $\eta(\beta) > 0$), so that the compressibilities satisfy $0 < \kappa_S < \kappa_{T_{\mathrm{eff}}}$.

To summarize, a necessary and sufficient condition for the inequalities $C_P > C_V > 0$ to hold is a positive effective temperature parameter β_{eff} with positive derivative $\beta'_{\mathrm{eff}}(\beta)$. In particular, $C_V > 0$ is equivalent to $\beta'_{\mathrm{eff}}(\beta) > 0$, and $C_P > C_V$ is equivalent to $\beta_{\mathrm{eff}}/\beta'_{\mathrm{eff}}(\beta) > 0$. The inequalities $0 < \kappa_S < \kappa_{T_{\mathrm{eff}}}$ with $\kappa_{T_{\mathrm{eff}}} = 1/P$ are equivalent to $\beta_{\mathrm{eff}} > 0$. A positive expansion coefficient α_{exp} in (3.24) is equivalent to $\beta'_{\mathrm{eff}}(\beta) > 0$.

4. Weibull decay of the spectral flux density of ultra-high energy cosmic-ray nuclei

In Sections 2 and 3, we have studied a general stationary non-equilibrium gas defined by a spectral number density $\mathrm{d}\rho/\mathrm{d}p$ structured as in (2.1). Here and in the next section, we discuss a concrete example, cosmic-ray nuclei constituting a relativistic gas mixture in stationary non-equilibrium. The flux density of this nuclear gas, based on number density (2.1), can be inferred from a spectral fit. In this section, we will perform the spectral fit, using flux data collected by several recent experiments covering the 1 GeV-10^{11} GeV interval, cf. Section 1, and find an analytic representation of the flux density and in particular of the power-law spectral function $h(p)$ in number density (2.1) which has been left unspecified so far.

The differential flux density per steradian defined by number density $\mathrm{d}\rho/\mathrm{d}p$ in (2.1) is $\mathrm{d}\Phi/\mathrm{d}p = \upsilon\mathrm{d}\rho/(4\pi\,\mathrm{d}p)$, with group velocity $\upsilon = p/E$ and dispersion relation $E = \sqrt{p^2+m^2}$. The spectral fit is performed with the rescaled flux density $F = p^\kappa \mathrm{d}\Phi/\mathrm{d}p$, cf. (2.1),

$$F = A_\Phi \frac{p^{3+\kappa}h(p)}{\sqrt{p^2+m^2}}\exp(-\beta(p^2+m^2)^{\sigma/2}), \tag{4.1}$$

with amplitude

$$A_\Phi = \frac{s\mathrm{e}^{-\alpha}}{(2\pi)^3}\frac{1}{c^2[\mathrm{m/s}]\hbar^3[\mathrm{GeV\,s}]} \approx 1.573\times 10^{53} s\,\mathrm{e}^{-\alpha}. \tag{4.2}$$

The units used are F $[(\mathrm{GeV}/c)^{\kappa-1}\mathrm{sr}^{-1}\mathrm{m}^{-2}\mathrm{s}^{-1}]$ and A_Φ $[(\mathrm{GeV}/c)^{-3}\mathrm{sr}^{-1}\mathrm{m}^{-2}\mathrm{s}^{-1}]$, cf. Section 2.1. The scale factor p^κ in (4.1) can be freely chosen, as it drops out in the χ^2 functional of the least squares fit. We use the scaling exponent $\kappa = 2.7$ to make spectral breaks of the flux density visible in log–log plots over the 1 GeV-10^{11} GeV interval. The number density (2.1) can be extracted from the fitted flux density, $\mathrm{d}\rho/\mathrm{d}p = 4\pi F(p)\sqrt{p^2+m^2}/p^{\kappa+1}$, cf. Section 5.1.

The all-particle flux density $F_{\rm all}$ of the nuclear gas in Fig. 1 is fitted with two partial fluxes of type (4.1), $F_{\rm all} = F_{\rm H,ext}+F_{\rm He,ext}$,

$$F_{\rm H,ext}(p) = A_{\Phi,\rm H}\frac{p^{3+\kappa}h_{\rm H,ext}(p)}{\sqrt{p^2+m_{\rm H}^2}}\exp(-\beta(p^2+m_{\rm H}^2)^{\sigma/2}), \tag{4.3}$$

where the spectral kernel $h_{\rm H,ext}$ is a multiply broken power law with smooth transitions at the spectral breaks,

$$h_{\rm H,ext}(p) = \frac{(1+(p/c_{2\rm H})^{\gamma_{2\rm H}/\delta_{2\rm H}})^{\delta_{2\rm H}}}{(1+(p/c_{1\rm H})^{\gamma_{1\rm H}/\delta_{1\rm H}})^{\delta_{1\rm H}}}\frac{1}{(1+(p/c_3)^{\gamma_3/\delta_3})^{\delta_3}}\frac{(1+(p/c_5)^{\gamma_5/\delta_5})^{\delta_5}}{(1+(p/c_4)^{\gamma_4/\delta_4})^{\delta_4}}\frac{(1+(p/c_7)^{\gamma_7/\delta_7})^{\delta_7}}{(1+(p/c_6)^{\gamma_6/\delta_6})^{\delta_6}}. \tag{4.4}$$

The second flux component $F_{\rm He,ext}$ and its spectral kernel $h_{\rm He,ext}$ are defined analogously, with the H subscript replaced by He. The positive amplitudes c_k (indexed in ascending order) in (4.4) determine the location of the spectral breaks, see Figs. 1 and 2. The exponents γ_k and δ_k are positive as well; the γ_k define the slopes of the spectral curve between the spectral breaks (which are nearly straight in double-logarithmic plots), and the δ_k determine the curvature of the spectral map at the spectral breaks c_k. The exponents and amplitudes of the spectral functions $h_{\rm H,ext}$ and $h_{\rm He,ext}$ obtained from the χ^2 fit are recorded in Table 1.

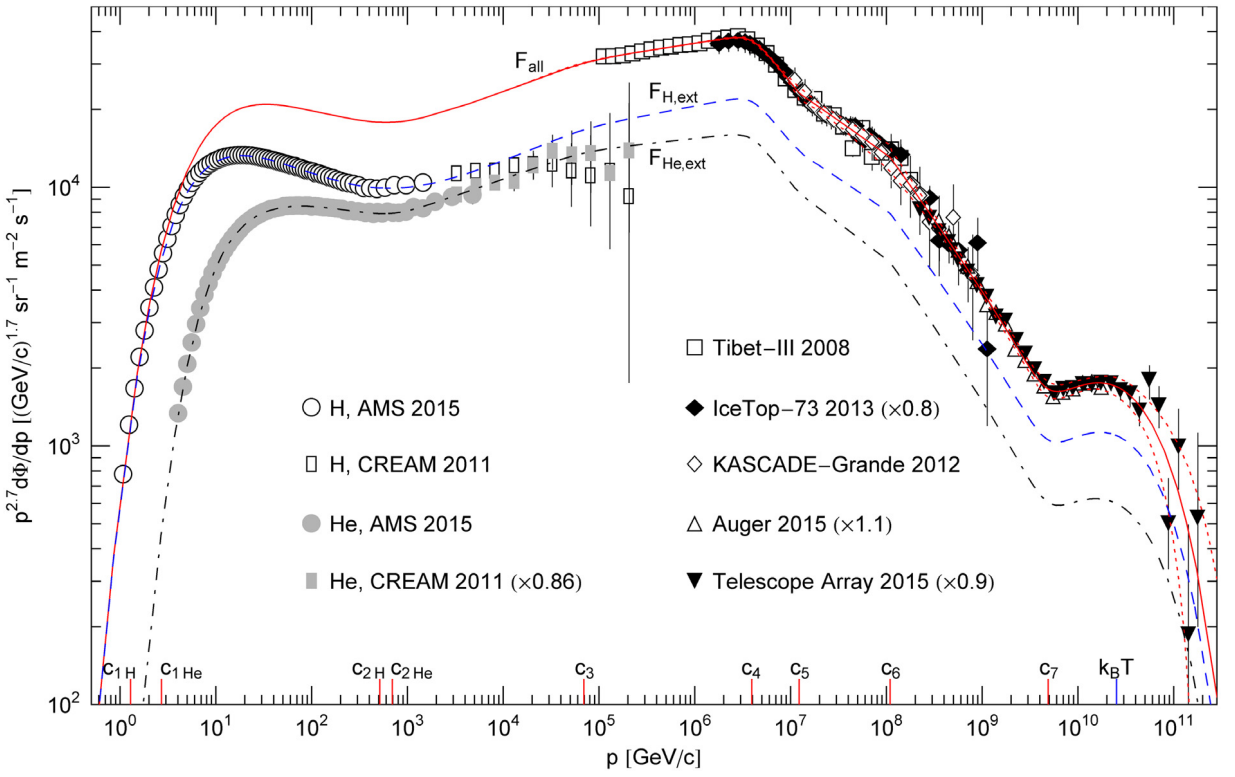

Fig. 1. Spectral fit to the all-particle flux of cosmic-ray nuclei in the 1 GeV−10^{11} GeV interval. Data points from AMS-02 [1,2], CREAM [3], Tibet-III [4], IceTop-73 (rescaled by a factor of 0.8) [5,6], KASCADE-Grande [7], Auger (rescaled by 1.1) [8] and Telescope Array (rescaled by 0.9) [9]. The rescaling is needed to obtain a continuous spectral curve. First, two independent χ^2 fits are performed to the hydrogen and helium flux points in the 1 GeV−10^4 GeV interval with the low-energy flux densities $F_{\rm H,\,low}$ and $F_{\rm He,\,low}$ in (4.5) (χ^2(H)/dof ≈ 15.1/68, χ^2(He)/dof ≈ 12.2/66). An approximation of the total flux is obtained by adding the hydrogen and helium fluxes, as the all-particle spectrum in this energy range consists predominantly of hydrogen and helium, $F_{\rm all,\,low} = F_{\rm H,\,low} + F_{\rm He,\,low}$. The flux density $F_{\rm all,\,low}$ is then analytically extended to higher energies as a multiply broken power law with Weibull spectral cutoff, $F_{\rm all} = F_{\rm H,ext} + F_{\rm He,ext}$, cf. (4.3) and (4.4), and a separate least-squares fit is performed to the all-particle flux points in the 10^5 GeV−10^{11} GeV interval with flux density $F_{\rm all}$ (solid curve, χ^2/dof ≈ 212/102). Also depicted are the partial fluxes $F_{\rm H,ext}$ and $F_{\rm He,ext}$ (dashed and dot-dashed curves, respectively), which are analytic extensions of the low-energy fluxes $F_{\rm H,\,low}$ and $F_{\rm He,\,low}$ in the 1 GeV−10^4 GeV interval, cf. (4.3)–(4.5). The dotted curves define the 3σ error band, better visible in Fig. 2. The fit parameters of the all-particle flux $F_{\rm all}$ are listed in Tables 1 and 2. The clearly visible spectral breaks (labeled c_k in Table 1) are indicated on the abscissa, as well as the cutoff temperature $k_{\rm B}T$ in the Weibull factor of the flux density, cf. (4.3).

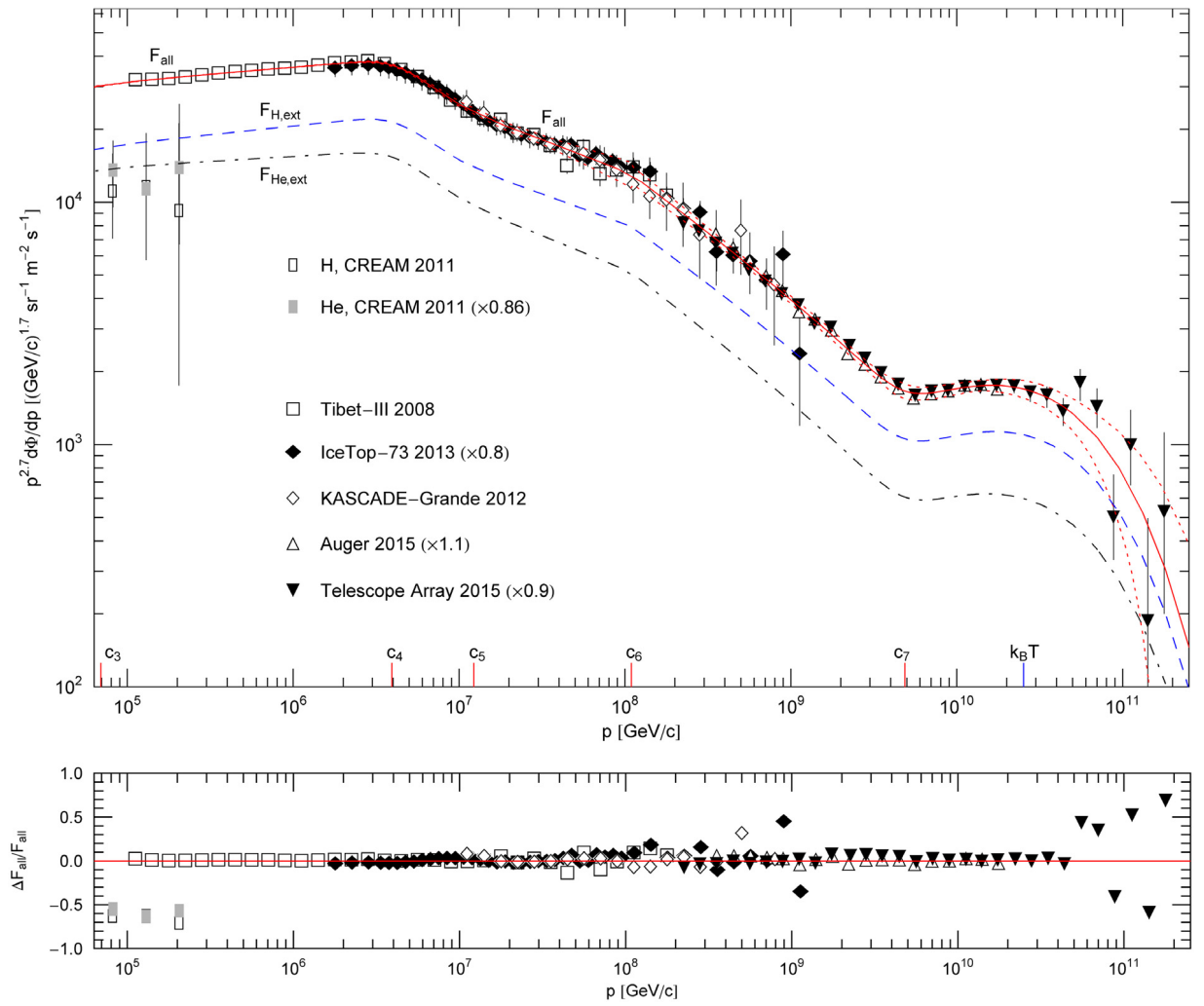

Fig. 2. Subexponential Weibull decay of the all-particle cosmic-ray spectrum. This is a close-up of Fig. 1; data points as in Fig. 1. Below the cutoff energy at $k_BT \approx 2.5 \times 10^{10}$ GeV, the flux density F_{all} (solid curve) is composed of multiple power-law segments (appearing approximately straight in log–log plots) with smooth transitions at the spectral breaks c_k, cf. Table 1. The subexponential spectral decay at ultra-high energies above k_BT is caused by the Weibull factor $\exp[-(p/(k_BT))^\sigma]$ in flux density (4.3). The spectral index is $\sigma \approx 0.66$, cf. Table 2, resulting in subexponential decay. The extensions $F_{H,ext}$ and $F_{He,ext}$ (dashed and dot-dashed curves) of the low-energy hydrogen and helium fluxes, cf. the caption to Fig. 1, contain admixtures of heavier nuclei (in the ultra-relativistic regime above 10^4 GeV) and add up to the all-particle flux, $F_{all} = F_{H,ext} + F_{He,ext}$, cf. (4.3) and (4.4). The 3σ error band is indicated by the dotted curves. The residuals of the least-squares fit of F_{all} are shown in the lower panel.

Table 1
Fitting parameters of the spectral functions $h_{H,ext}(p)$ and $h_{He,ext}(p)$ of the extended hydrogen and helium fluxes $F_{H,ext}$, $F_{He,ext}$ in Figs. 1 and 2. The spectral functions are multiply broken power laws stated in (4.4). The power-law amplitudes c_k define the location of the spectral breaks, see Fig. 1. The exponents γ_k determine the spectral slopes between the breaks, and the exponents δ_k the spectral curvature at the break points.

k	c_k [GeV/c]	γ_k	δ_k
1H	1.283	4.910	4.125
2H	5.128×10^2	0.3709	0.3698
1He	2.694	4.775	3.848
2He	6.955×10^2	0.2045	6.409×10^{-2}
3	6.925×10^4	8.857×10^{-2}	3.091×10^{-2}
4	3.935×10^6	0.5185	8.622×10^{-2}
5	1.227×10^7	0.2067	3.182×10^{-3}
6	1.091×10^8	0.2463	2.193×10^{-3}
7	4.866×10^9	0.9946	0.1957

Table 2
Flux amplitudes and decay parameters. $A_{\Phi,\mathrm{H}}$ and $A_{\Phi,\mathrm{He}}$ denote the amplitudes of the partial fluxes $F_{\mathrm{H,ext}}$, $F_{\mathrm{He,ext}}$ in (4.3). The subexponential spectral decay of the flux components is determined by the Weibull factor $\exp(-\beta p^\sigma)$, where σ is the spectral index and β the decay exponent related to the cutoff temperature by $\beta = 1/(k_{\mathrm{B}}T)^\sigma$. (The mass-square in the Weibull factor in (4.3) can be dropped because of the high cutoff temperature.)

$A_{\Phi,\mathrm{H}}$ [$(\mathrm{GeV}/c)^{-3}\,\mathrm{sr}^{-1}\,\mathrm{m}^{-2}\,\mathrm{s}^{-1}$]	$A_{\Phi,\mathrm{He}}$ [$(\mathrm{GeV}/c)^{-3}\,\mathrm{sr}^{-1}\,\mathrm{m}^{-2}\,\mathrm{s}^{-1}$]	$k_{\mathrm{B}}T$ [GeV]	σ	β [$\mathrm{GeV}^{-\sigma}$]
$(8.428 \pm 1.6) \times 10^3$	$(1.095 \pm 0.20) \times 10^2$	$(2.529 \pm 0.070) \times 10^{10}$	0.6645 ± 0.014	1.223×10^{-7}

The power-law function (4.4) is an example of how wideband spectra exhibiting extended spectral slopes and multiple spectral breaks [45–49] can systematically be assembled. First, one visually determines the approximate location of the spectral breaks c_k in a double-logarithmic plot of the data sets. (The break points c_k are the joints of spectral slopes, as indicated on the abscissa of Figs. 1 and 2.) These preliminary c_k are used as initial guess in the least square fit, and they determine the number of factors in the spectral function $\prod_k(1+(p/c_k)^{\gamma_k/|\delta_k|})^{\delta_k}$. (In this product notation, we use negative exponents δ_k for the factors in the denominator of (4.4).) Initial guesses for the exponents γ_k and the sign of δ_k can be read off from the ascending or descending spectral slopes. A moderate exponent δ_k results in a gradual change of the slope at the spectral break c_k, and a δ_k close to zero causes a sudden break in the spectral map. Each spectral break is thus determined by three parameters, the location of the break points c_k, the power-law index γ_k of one adjacent slope, and the curvature exponent δ_k. The power-law function (4.4) describes seven spectral breaks specified by 21 parameters. To locate the spectral breaks in the flux map, it is also necessary to rescale the flux data, to make the spectral fine structure visible. This is done in Figs. 1 and 2 by multiplying the spectral flux density by a factor of $p^{2.7}$. In the unscaled flux representation of Fig. 3, which is also a log–log plot, the fine structure is largely concealed.

The partial flux $F_{\mathrm{H,ext}}(p)$ in (4.3) is the extension of the low-energy (1 GeV–10^4 GeV) hydrogen component of the all-particle spectrum defined by the AMS-02 [1,2] and CREAM [3] hydrogen flux points in Fig. 1,

$$F_{\mathrm{H,\,low}}(p) = \frac{A_{\Phi,\mathrm{H}}p^{3+\kappa}}{\sqrt{p^2+m_{\mathrm{H}}^2}}\,\frac{(1+(p/c_{2\mathrm{H}})^{\gamma_{2\mathrm{H}}/\delta_{2\mathrm{H}}})^{\delta_{2\mathrm{H}}}}{(1+(p/c_{1\mathrm{H}})^{\gamma_{1\mathrm{H}}/\delta_{1\mathrm{H}}})^{\delta_{1\mathrm{H}}}}. \tag{4.5}$$

Analogously, $F_{\mathrm{He,ext}}$ is the extension of the low-energy helium flux $F_{\mathrm{He,\,low}}$ defined by the AMS-02 and CREAM helium flux points in Fig. 1; $F_{\mathrm{He,\,low}}(p)$ is parametrized as in (4.5), with the H subscript replaced by He. We use $m_{\mathrm{H}} \approx 0.938$ GeV as proton mass and $m_{\mathrm{He}} \approx 3.727$ GeV for alpha particles. The amplitudes $A_{\Phi,\mathrm{H}}$ and $A_{\Phi,\mathrm{He}}$ in (4.3) and (4.5) are related to the fugacity parameters α_{H} and α_{He} as stated in (4.2), with spin degeneracy $s_{\mathrm{H}} = 2$ for protons and $s_{\mathrm{He}} = 1$ for alpha particles. In the Weibull factor in (4.3), we can drop the mass term, using $\exp(-\beta p^\sigma)$ instead, as the spectral cutoff happens at very high momentum in the ultra-relativistic regime where the nuclear mass is negligible, see the spectral cutoff depicted in Fig. 2. The amplitudes $A_{\Phi,\mathrm{H}}$ and $A_{\Phi,\mathrm{He}}$ as well as the decay exponent $\beta = 1/(k_{\mathrm{B}}T)^\sigma$ and the spectral index σ of the Weibull factor, cf. Section 2.1, are fitting parameters listed in Table 2.

The spectral fit is performed in two steps. First, we fit the hydrogen and helium components, in the low-energy interval from 1 GeV to 10^4 GeV, using the AMS-02 and CREAM data sets and the low-energy limit (4.5). In this way, we obtain the flux amplitude $A_{\Phi,\mathrm{H}}$, the power-law amplitudes $c_{1\mathrm{H}}$, $c_{2\mathrm{H}}$ and the exponents $\gamma_{1\mathrm{H}}$, $\gamma_{2\mathrm{H}}$ and $\delta_{1\mathrm{H}}$, $\delta_{2\mathrm{H}}$, and analogously for the helium fit. In the 1 GeV–10^4 GeV interval, the all-particle flux consists mainly of hydrogen and helium nuclei; heavier nuclei contribute only around one percent to the total flux in this interval, so that the all-particle flux in this energy range can be approximated by $F_{\mathrm{all}} \sim F_{\mathrm{H,low}} + F_{\mathrm{He,low}}$.

The second step is to fit the high-energy all-particle spectrum in the 10^5 GeV-10^{11} GeV interval as defined by the Tibet-III [4], IceTop-73 [5,6], KASCADE-Grande [7], Auger [8] and Telescope Array [9] flux points in Figs. 1 and 2. To this end, we extend the low-energy fit $F_{\mathrm{H,low}} + F_{\mathrm{He,low}}$ to higher energies, by adding power-law factors to the spectral kernels $h_{\mathrm{H,low}}(p)$ and $h_{\mathrm{He,low}}(p)$ as done in (4.4). The added power-law factors are the same for both kernels, with amplitudes $c_{k=3,\ldots,7}$ and exponents γ_k, δ_k listed in Table 1. The high-energy flux extensions $F_{\mathrm{H,ext}}$ and $F_{\mathrm{He,ext}}$ above 10^4 GeV also contain heavier nuclei, an intermediate-mass nitrogen-like component and a heavy iron-like component. At ultra-relativistic energies above 10^4 GeV, the nuclear rest mass is negligible since $m^2/p^2 \ll 1$, so that heavier nuclei can be accommodated in the hydrogen and helium flux extensions. The spectral breaks c_k indicated on the abscissa of Figs. 1 and 2 are clearly discernible in the total flux $F_{\mathrm{all}} = F_{\mathrm{H,ext}} + F_{\mathrm{He,ext}}$ and the partial fluxes. The Weibull factor with spectral index $\sigma = 0.66 \pm 0.02$ in flux density (4.3) generates the subexponential spectral cutoff in the ultra-high energy regime above the 'ankle' $c_7 \approx 4.9 \times 10^9$ GeV of the all-particle spectrum, cf. Fig. 2; another major spectral break occurs at the 'knee' $c_4 \approx 3.9 \times 10^6$ GeV, cf. Refs. [10,50].

5. Cosmic-ray nuclei: a relativistic gas mixture in stationary non-equilibrium

5.1. Reduction to a two-component mixture: spectral extension of the low-energy hydrogen and helium components

The following discussion is a step-by-step adaptation of the thermodynamic formalism developed in Section 3 (for a one-component gas in stationary non-equilibrium) to cosmic-ray nuclei, which constitute a gas mixture because of the different particle masses. In Section 4, we have represented the empirical flux density of the all-particle cosmic-ray spectrum as the sum of two partial fluxes, $F_{\mathrm{all}} = F_{\mathrm{H,ext}} + F_{\mathrm{He,ext}}$, which are extensions of the low-energy hydrogen and helium fluxes, cf. (4.3) and (4.5). Heavier nuclei have been included in these two extensions, since the all-particle spectrum below 10^4 GeV is predominantly composed of protons and helium, and above 10^4 GeV, the flux densities are mass independent. In effect, the

all-particle flux density $F_{\rm all}$ depends only on the proton and helium mass, and can therefore be treated as a two-component mixture.

As pointed out after (4.2), the differential number density $\mathrm{d}\rho_{\rm H,ext}$ can be inferred from the flux density $F_{\rm H,ext}$ (obtained from the spectral fit described in Section 4, cf. (4.3) and (4.4) and Tables 1 and 2),

$$\mathrm{d}\rho_{\rm H,ext}\,[\mathrm{m}^{-3}] = \frac{4\pi}{c\,[\mathrm{m/s}]}F_{\rm H,ext}(p)\frac{\sqrt{p^2+m_{\rm H}^2}}{p^{1+\kappa}}\mathrm{d}p. \tag{5.1}$$

The partition function defined by this number density is $\log Z_{\rm H,ext} = V\int_0^\infty \mathrm{d}\rho_{\rm H,ext}(p)$, cf. (2.3). The same holds for the helium extension $F_{\rm He,ext}$, $\mathrm{d}\rho_{\rm He,ext}$, $\log Z_{\rm He,ext}$, with the H subscript replaced by He. The partial number densities $\mathrm{d}\rho_{\rm H,ext}/\mathrm{d}p$, $\mathrm{d}\rho_{\rm He,ext}/\mathrm{d}p$ and their sum $\mathrm{d}\rho_{\rm all}/\mathrm{d}p$ (number density of the all-particle flux $F_{\rm all}$) are depicted in Fig. 3. They consist of an ascending power-law slope (straight in log–log plots), a spectral peak at around 1 GeV, a descending power-law slope extending to the cutoff temperature $k_{\rm B}T \approx 2.5\times 10^{10}$ GeV, and a subexponential Weibull tail with spectral index $\sigma \approx 0.66$, cf. Section 2.1. The power-law descent contains multiple spectral breaks indicated on the abscissa of Fig. 3, which are better visible in the rescaled flux maps of Figs. 1 and 2.

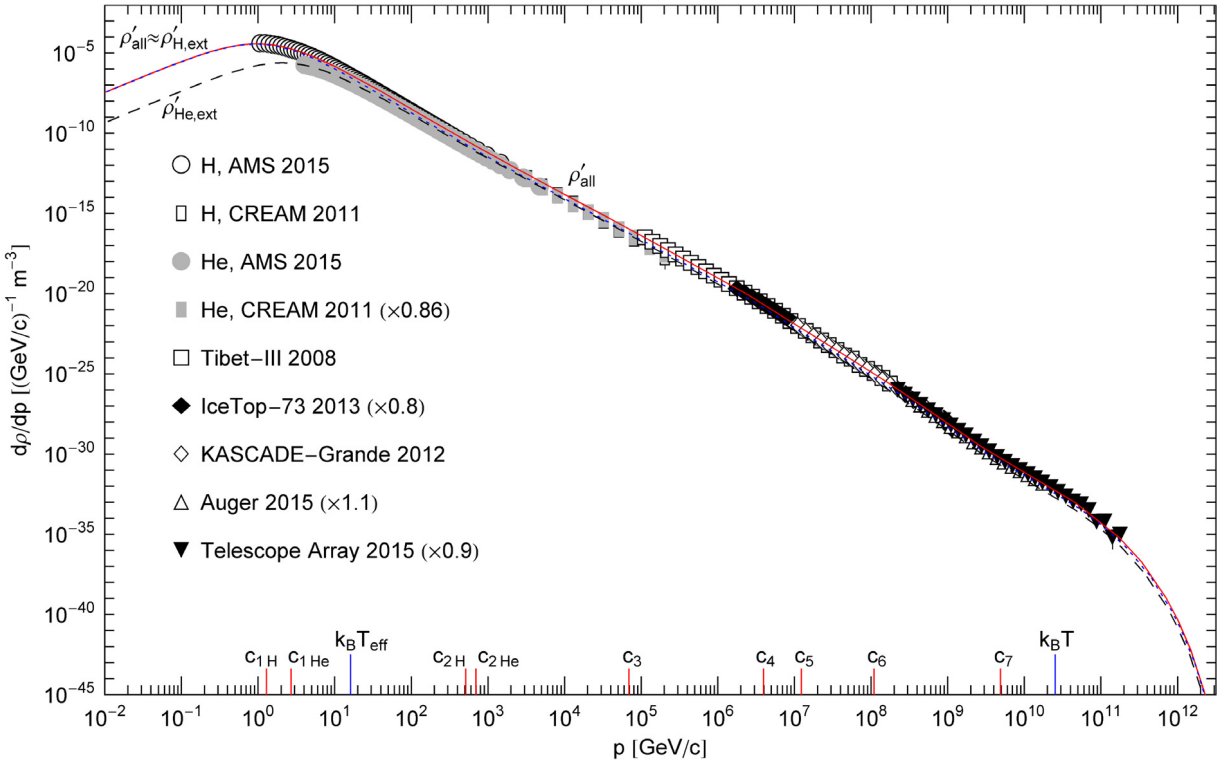

Fig. 3. Spectral number density of cosmic-ray nuclei. Data points as in Fig. 1. The differential number density $\mathrm{d}\rho_{\rm all}/\mathrm{d}p$ (solid curve $\rho'_{\rm all}$) of the nuclear gas is the sum of two partial densities, $\rho'_{\rm all}(p) = \rho'_{\rm H,ext} + \rho'_{\rm He,ext}$; the scale factor $p^{2.7}$ used in the plots of the corresponding partial fluxes $F_{\rm H,\,ext}$ and $F_{\rm He,\,ext}$ in Figs. 1 and 2 has been dropped in this figure. As the helium extension $\rho'_{\rm He,ext}$ (dashed curve) is by about one order lower than the hydrogen extension $\rho'_{\rm H,ext}$ (dotted), the total density $\rho'_{\rm all}$ is nearly indistinguishable from $\rho'_{\rm H,ext}$ in this unscaled representation. The partial number densities $\rho'_{\rm H,ext}$, $\rho'_{\rm He,ext}$ are extracted from the flux densities $F_{\rm H,\,ext}$, $F_{\rm He,\,ext}$ in Figs. 1 and 2 by way of Eq. (5.1). In the interval between the spectral peak and the subexponential spectral cutoff at $k_{\rm B}T \approx 2.5\times 10^{10}$ GeV, the number density appears as nearly straight power-law slope in this representation, despite of multiple spectral breaks indicated on the abscissa. Discounting these breaks, $\rho'_{\rm all}$ has a simple structure: a power-law ascent, a spectral peak at around 1 GeV, an extended power-law descent, and a subexponential spectral tail above the cutoff temperature $k_{\rm B}T$. Also indicated on the abscissa is the effective temperature $k_{\rm B}T_{\rm eff} \approx 16$ GeV of the nuclear gas, cf. (5.10) and Table 3.

As in Section 3.1, the partition factor of the hydrogen spectral extension $\mathrm{d}\rho_{\rm H,ext}$ is defined by

$$z_{\rm H}(\beta,\gamma,\delta,\varepsilon)\,[\mathrm{m}^{-3}] = \int_0^\infty \mathrm{d}\hat\rho_{\rm H}(p), \tag{5.2}$$

with spectral measure, cf. (2.2) and (3.1),

$$\mathrm{d}\hat\rho_{\rm H}(p) = \frac{4\pi s_{\rm H}}{(2\pi\hbar c)^3}\exp[-\beta(p^2+m_{\rm H}^2)^{\sigma/2} - \gamma\log\frac{1}{h_{\rm H,ext}(p)} - \delta\frac{1}{3}\frac{p^2}{\sqrt{p^2+m_{\rm H}^2}} - \varepsilon\sqrt{p^2+m_{\rm H}^2}]p^2\mathrm{d}p. \tag{5.3}$$

$h_{\mathrm{H,ext}}(p)$ is the power-law spectral function (4.4), m_{H} the proton mass and s_{H} the spin degeneracy, cf. after (4.5). The partition factor z_{H} and derivatives thereof are taken at $\gamma = 1, \delta = \varepsilon = 0$, see Section 3.1, so that z_{H} only depends on the decay exponent β. At $\gamma = 1, \delta = \varepsilon = 0$, we find $\mathrm{d}\hat{\rho}_{\mathrm{H}} = \mathrm{d}\rho_{\mathrm{H,ext}}/f_{\mathrm{H}}$ and $z_{\mathrm{H}} = \log Z_{\mathrm{H,ext}}/(Vf_{\mathrm{H}})$, where $f_{\mathrm{H}} = \mathrm{e}^{-\alpha_{\mathrm{H}}}$ denotes the fugacity, cf. (4.2) and after (4.5). The units stated after (2.1) are used, z_{H} [m^{-3}].

The number count, internal energy and pressure of the hydrogenic partial flux $F_{\mathrm{H,ext}}$ can thus be calculated as $N_{\mathrm{H}} = V\mathrm{e}^{-\alpha_{\mathrm{H}}}z_{\mathrm{H}}$, $U_{\mathrm{H}} = -V\mathrm{e}^{-\alpha_{\mathrm{H}}}z_{\mathrm{H},\varepsilon}$, $P_{\mathrm{H}} = -\mathrm{e}^{-\alpha_{\mathrm{H}}}z_{\mathrm{H},\delta}$, and the Weibull and excess entropies read $W_{\mathrm{H}}/\beta = -V\mathrm{e}^{-\alpha_{\mathrm{H}}}z_{\mathrm{H},\beta}$ and $H_{\mathrm{H}} = -V\mathrm{e}^{-\alpha_{\mathrm{H}}}z_{\mathrm{H},\gamma}$, cf. Section 2.2; α_{H} is the fugacity parameter of the hydrogen component. This also holds for the helium extension $F_{\mathrm{He,ext}}$ with subscript H replaced by He in (5.2) and (5.3). The respective quantities of the all-particle flux F_{all} are obtained by addition, $N = N_{\mathrm{H}} + N_{\mathrm{He}}$, $W = W_{\mathrm{H}} + W_{\mathrm{He}}$, etc. In this way, we find the $(\alpha_{\mathrm{H}}, \alpha_{\mathrm{He}}, \beta, V)$ parametrization of the thermodynamic variables. The entropy is assembled as $S(\alpha_{\mathrm{H}}, \alpha_{\mathrm{He}}, \beta, V) = S_{\mathrm{H}} + S_{\mathrm{He}}$, where, cf. (3.4),

$$S_{\mathrm{H}}(\alpha_{\mathrm{H}}, \beta, V) = V\mathrm{e}^{-\alpha_{\mathrm{H}}}((1+\alpha_{\mathrm{H}})z_{\mathrm{H}} - \beta z_{\mathrm{H},\beta} - z_{\mathrm{H},\gamma}), \tag{5.4}$$

and analogously $S_{\mathrm{He}}(\alpha_{\mathrm{He}}, \beta, V)$.

When calculating thermodynamic variables from spectral fits, the (α, β, V) parametrization is the most efficient representation. The variables N, U, S, W, H and P listed in the first row of Table 3 are assembled as stated after (5.3). The partition factor z_{H} in (5.2) and its derivatives, cf. after (3.1), are calculated with the spectral measure $\mathrm{d}\hat{\rho}_{\mathrm{H}} = \mathrm{d}\rho_{\mathrm{H,ext}}/f_{\mathrm{H}}$ obtained from the hydrogenic flux extension $F_{\mathrm{H,ext}}$ by way of (5.1). The analytic flux density $F_{\mathrm{H,ext}}$ is stated in (4.3) and (4.4), with fit parameters in Tables 1 and 2. The fugacity f_{H} is calculated from the flux amplitude in (4.2) and Table 2. Analogously for the partition factor z_{He} of the helium component.

Table 3
Thermodynamic parameters of the all-particle spectrum of cosmic-ray nuclei, a relativistic gas mixture in stationary non-equilibrium. The spectral number density of the nuclei is depicted in Fig. 3. Recorded in the first row: particle count N, internal energy U, total entropy S, Weibull entropy W, excess entropy H, pressure P, isochoric heat capacity C_V, and isobaric heat capacity C_P. These quantities are listed as specific densities rescaled with the volume factor and the Boltzmann constant k_{B}. The calculation of the variables N, U, S, W, H and P is explained in Section 5.1. The heat capacities C_V and C_P are assembled as stated in (5.15) and (5.21). Quantities recorded in the second row: isothermal compressibility $\kappa_{T_{\mathrm{eff}}}$, cf. after (5.22), adiabatic compressibility κ_S, cf. (5.27), heat capacity ratio C_P/C_V coinciding with the compressibility ratio $\kappa_{T_{\mathrm{eff}}}/\kappa_S$, cf. after (5.27), isobaric expansion coefficient α_{exp}, cf. (5.23), effective temperature parameter $\beta_{\mathrm{eff}} = 1/(k_{\mathrm{B}}T_{\mathrm{eff}})$, cf. (5.10), effective temperature T_{eff}, and the equipartition ratio $U/(Nk_{\mathrm{B}}T_{\mathrm{eff}})$.

N/V [m^{-3}]	U/V [GeV m^{-3}]	$S/(k_{\mathrm{B}}V)$ [m^{-3}]	$W/(k_{\mathrm{B}}V)$ [m^{-3}]	$H/(k_{\mathrm{B}}V)$ [m^{-3}]	P [GeV m^{-3}]	$C_V/(k_{\mathrm{B}}V)$ [m^{-3}]	$C_P/(k_{\mathrm{B}}V)$ [m^{-3}]
1.238×10^{-4}	5.935×10^{-4}	1.490×10^{-2}	3.741×10^{-11}	5.937×10^{-4}	1.705×10^{-4}	6.271×10^{-9}	3.083×10^{-8}

$\kappa_{T_{\mathrm{eff}}}$ [GeV^{-1} m^3]	κ_S [GeV^{-1} m^3]	C_P/C_V, $\kappa_{T_{\mathrm{eff}}}/\kappa_S$	$\alpha_{\mathrm{exp}}/k_{\mathrm{B}}$ [GeV^{-1}]	β_{eff} [GeV^{-1}]	$k_{\mathrm{B}}T_{\mathrm{eff}}$ [GeV]	T_{eff} [K]	$U/(Nk_{\mathrm{B}}T_{\mathrm{eff}})$
5.866×10^3	1.193×10^3	4.915	1.233×10^{-5}	6.216×10^{-2}	16.09	1.867×10^{14}	0.2981

5.2. Thermal equation of state of a stationary non-equilibrium mixture

To obtain the thermodynamic variables in $(\beta, V, N_{\mathrm{H}}, N_{\mathrm{He}})$ parametrization, we invert the number count, $\alpha_{\mathrm{H}} = \log(z_{\mathrm{H}}V/N_{\mathrm{H}})$, and substitute the fugacity parameter α_{H}, cf. after (5.3). The hydrogen component of the internal energy then reads

$$U_{\mathrm{H}}(\beta, N_{\mathrm{H}}) = N_{\mathrm{H}}u_{\mathrm{H}}(\beta), \quad u_{\mathrm{H}}(\beta) = -\frac{z_{\mathrm{H},\varepsilon}}{z_{\mathrm{H}}}, \tag{5.5}$$

and analogously the helium component $U_{\mathrm{He}}(\beta, N_{\mathrm{He}})$. The total internal energy of the mixture is thus

$$U = \hat{u}(\beta, N_{\mathrm{H}}, N_{\mathrm{He}}), \quad \hat{u}(\beta, N_{\mathrm{H}}, N_{\mathrm{He}}) = N_{\mathrm{H}}u_{\mathrm{H}}(\beta) + N_{\mathrm{He}}u_{\mathrm{He}}(\beta). \tag{5.6}$$

The partial pressures and the thermal equation of state read

$$P_{\mathrm{H}} = \frac{N_{\mathrm{H}}}{V}\eta_{\mathrm{H}}(\beta), \quad \eta_{\mathrm{H}}(\beta) = -\frac{z_{\mathrm{H},\delta}(\beta)}{z_{\mathrm{H}}(\beta)},$$

$$P = \frac{1}{V}\hat{\eta}(\beta, N_{\mathrm{H}}, N_{\mathrm{He}}), \quad \hat{\eta}(\beta, N_{\mathrm{H}}, N_{\mathrm{He}}) = N_{\mathrm{H}}\eta_{\mathrm{H}}(\beta) + N_{\mathrm{He}}\eta_{\mathrm{He}}(\beta). \tag{5.7}$$

The entropy variable $S(\beta, V, N_{\mathrm{H}}, N_{\mathrm{He}})$ is assembled as

$$S = N_{\mathrm{H}}\left(1 - \log\frac{N_{\mathrm{H}}}{V}\right) + N_{\mathrm{He}}\left(1 - \log\frac{N_{\mathrm{He}}}{V}\right) + \hat{s}(\beta, N_{\mathrm{H}}, N_{\mathrm{He}}),$$
$$\hat{s}(\beta, N_{\mathrm{H}}, N_{\mathrm{He}}) = N_{\mathrm{H}}s_{\mathrm{H}}(\beta) + N_{\mathrm{He}}s_{\mathrm{He}}(\beta), \tag{5.8}$$

where $s_{\mathrm{H}}(\beta)$ and $s_{\mathrm{He}}(\beta)$ are defined in (3.7), with the partition factor z indexed z_{H} and z_{He}, respectively.

5.3. Effective temperature and chemical potential of cosmic-ray nuclei

To calculate the effective gas temperature, we need the $(U, V, N_{\rm H}, N_{\rm He})$ parametrization of entropy. Inversion of the internal energy in (5.6) and substitution of $\beta = \hat{u}^{-1}(U, N_{\rm H}, N_{\rm He})$ into (5.8) gives

$$S(U, V, N_{\rm H}, N_{\rm He}) = N_{\rm H}\left(1 - \log\frac{N_{\rm H}}{V}\right) + N_{\rm He}\left(1 - \log\frac{N_{\rm He}}{V}\right) + \hat{s}(\hat{u}^{-1}(U, N_{\rm H}, N_{\rm He}), N_{\rm H}, N_{\rm He}). \tag{5.9}$$

The effective temperature parameter $\beta_{\rm eff} = 1/(k_{\rm B}T_{\rm eff})$ of the gas mixture is defined by the entropy derivative

$$S_{,U} = \frac{\hat{s}_{,\beta}(\beta, N_{\rm H}, N_{\rm He})}{\hat{u}_{,\beta}(\beta, N_{\rm H}, N_{\rm He})} = \beta_{\rm eff},$$

$$\hat{u}_{,\beta} = N_{\rm H}u'_{\rm H}(\beta) + N_{\rm He}u'_{\rm He}(\beta), \quad \hat{s}_{,\beta} = N_{\rm H}s'_{\rm H}(\beta) + N_{\rm He}s'_{\rm He}(\beta). \tag{5.10}$$

The derivatives denoted by a prime are stated in (3.11), with z indexed $z_{\rm H}$ or $z_{\rm He}$. The effective fugacity parameter of the hydrogen extension $F_{\rm H,ext}$ is defined by the derivative

$$S_{,N_{\rm H}} = -\log\frac{N_{\rm H}}{V} - u_{\rm H}(\beta)\beta_{\rm eff} + s_{\rm H}(\beta) = \alpha^{\rm H}_{\rm eff}, \tag{5.11}$$

where we used $\hat{u}^{-1}_{,N_{\rm H}} = -\hat{u}_{,N_{\rm H}}/\hat{u}_{,\beta}$ and $\hat{u}_{,N_{\rm H}} = u_{\rm H}(\beta), \hat{s}_{,N_{\rm H}} = s_{\rm H}(\beta)$. The effective chemical potential of the nuclei constituting the flux component $F_{\rm H,ext}$ is $\mu^{\rm H}_{\rm eff} = -\alpha^{\rm H}_{\rm eff}/\beta_{\rm eff}$. The effective fugacity parameter $\alpha^{\rm He}_{\rm eff}$ and chemical potential $\mu^{\rm He}_{\rm eff}$ of the helium extension $F_{\rm He,ext}$ are obtained analogously. The effective temperature parameter is calculated by way of (5.10) and (3.11), using the spectral representation of the partition factors $z_{\rm H,He}$ in (5.2): $\beta_{\rm eff} \approx 6.216 \times 10^{-2}$/GeV. For the chemical potentials, we use (5.11) with $s_{\rm H}(\beta)$ in (3.7), $u_{\rm H}(\beta)$ in (5.5) and $N_{\rm H}/V$ as stated after (5.3) to estimate $\mu^{\rm H}_{\rm eff} \approx -1.910 \times 10^3$ GeV and, in like manner, $\mu^{\rm He}_{\rm eff} \approx -1.962 \times 10^3$ GeV.

5.4. Caloric equation of state and isochoric heat capacity of the nuclear gas

We switch to the $(\beta_{\rm eff}, V, N_{\rm H}, N_{\rm He})$ parametrization. By inverting $\beta_{\rm eff}$ in (5.10), $\beta = \beta(\beta_{\rm eff}, N_{\rm H}, N_{\rm He})$, and substituting into (5.6), we find the caloric equation of state

$$U(\beta_{\rm eff}, N_{\rm H}, N_{\rm He}) = \hat{u}(\beta(\beta_{\rm eff}, N_{\rm H}, N_{\rm He}), N_{\rm H}, N_{\rm He}). \tag{5.12}$$

We also note the thermal equation in this representation, cf. (5.7),

$$P = \frac{1}{V}\hat{\eta}(\beta(\beta_{\rm eff}, N_{\rm H}, N_{\rm He}), N_{\rm H}, N_{\rm He}), \tag{5.13}$$

and the entropy, cf. (5.8),

$$S(\beta_{\rm eff}, V, N_{\rm H}, N_{\rm He}) = N_{\rm H}(1 - \log\frac{N_{\rm H}}{V}) + N_{\rm He}(1 - \log\frac{N_{\rm He}}{V}) + \hat{s}(\beta(\beta_{\rm eff}, N_{\rm H}, N_{\rm He}), N_{\rm H}, N_{\rm He}). \tag{5.14}$$

The isochoric heat capacity $C_V = T_{\rm eff}S_{,T_{\rm eff}}(\beta_{\rm eff}, V, N_{\rm H}, N_{\rm He})$ reads

$$C_V = -\beta_{\rm eff}S_{,\beta_{\rm eff}}(\beta_{\rm eff}, V, N_{\rm H}, N_{\rm He}) = -\beta^2_{\rm eff}\frac{\hat{u}_{,\beta}}{\beta_{{\rm eff},\beta}}. \tag{5.15}$$

The β derivative of the effective temperature parameter $\beta_{\rm eff}(\beta, N_{\rm H}, N_{\rm He})$ is assembled as

$$\beta_{{\rm eff},\beta} = (\hat{s}_{,\beta,\beta} - \hat{u}_{,\beta,\beta}\beta_{\rm eff})/\hat{u}_{,\beta},$$
$$\hat{u}_{,\beta,\beta} = N_{\rm H}u''_{\rm H}(\beta) + N_{\rm He}u''_{\rm He}(\beta), \quad \hat{s}_{,\beta,\beta} = N_{\rm H}s''_{\rm H}(\beta) + N_{\rm He}s''_{\rm He}(\beta), \tag{5.16}$$

with $\beta_{\rm eff}$ and $\hat{u}_{,\beta}$ in (5.10). The primed second derivatives are calculated as stated in (3.15), with z indexed $z_{\rm H}$ and $z_{\rm He}$, respectively, cf. (5.2). $\hat{u}_{,\beta}$ in (5.10) is negative, since $u'_{\rm H,He}(\beta) < 0$, see Section 3.8; the derivatives $u'_{\rm H,He}(\beta)$ defining $\hat{u}_{,\beta}$ are calculated via (3.11) and (5.2). Positivity of C_V is thus assured by $\beta_{{\rm eff},\beta} > 0$. Using (5.16), we find $\beta_{{\rm eff},\beta}(\beta, N_{\rm H}, N_{\rm He}) \approx 7.010 \times 10^3\ {\rm GeV}^{\sigma-1}$, where σ is the Weibull spectral index, cf. after (2.1). The isochoric specific heat C_V listed in Table 3 is calculated by way of (5.15).

5.5. Isobaric heat capacity, isothermal compressibility and isobaric expansion coefficient of the nuclear gas

The $(\beta_{\rm eff}, P, N_{\rm H}, N_{\rm He})$ parametrization is used in this section. By way of the thermal equation (5.13), we find the volume factor $V(\beta_{\rm eff}, P, N_{\rm H}, N_{\rm He})$. The internal energy $U(\beta_{\rm eff}, N_{\rm H}, N_{\rm He})$ in (5.12) remains unchanged, as it does not depend on the volume factor. The entropy $S(\beta_{\rm eff}, P, N_{\rm H}, N_{\rm He})$ is found by eliminating V in (5.14) via the thermal equation,

$$S = (N_{\rm H} + N_{\rm He})(1 - \log P) + \hat{g}(\beta(\beta_{\rm eff}, N_{\rm H}, N_{\rm He}), N_{\rm H}, N_{\rm He}),$$

$$\hat{g}(\beta, N_{\rm H}, N_{\rm He}) = \hat{s} + N_{\rm H}\log\frac{\hat{\eta}}{N_{\rm H}} + N_{\rm He}\log\frac{\hat{\eta}}{N_{\rm He}}. \tag{5.17}$$

The $\beta_{\rm eff}$ derivative thereof reads

$$S_{,\beta_{\rm eff}}(\beta_{\rm eff}, P, N_{\rm H}, N_{\rm He}) = \frac{\hat{g}_{,\beta}}{\beta_{{\rm eff},\beta}} = S_{,\beta_{\rm eff}}(\beta_{\rm eff}, V, N_{\rm H}, N_{\rm He}) + \frac{N_{\rm H}+N_{\rm He}}{\beta_{{\rm eff},\beta}}\frac{\hat{\eta}_{,\beta}}{\hat{\eta}}, \tag{5.18}$$

with $S_{,\beta_{\rm eff}}(\beta_{\rm eff}, V, N_{\rm H}, N_{\rm He})$ as in (5.15). We also note the derivatives

$$\hat{g}_{,\beta}(\beta, N_{\rm H}, N_{\rm He}) = \beta_{\rm eff}\hat{u}_{,\beta} + (N_{\rm H}+N_{\rm He})\frac{\hat{\eta}_{,\beta}}{\hat{\eta}}, \tag{5.19}$$

$$\hat{\eta}_{,\beta}(\beta, N_{\rm H}, N_{\rm He}) = N_{\rm H}\eta'_{\rm H}(\beta) + N_{\rm He}\eta'_{\rm He}(\beta), \tag{5.20}$$

with $\eta'_{\rm H,He}(\beta)$ in (3.21). In this way, we can assemble the isobaric specific heat $C_P = T_{\rm eff}S_{,T_{\rm eff}}(\beta_{\rm eff}, P, N_{\rm H}, N_{\rm He})$ as

$$C_P = -\beta_{\rm eff}S_{,\beta_{\rm eff}}(\beta_{\rm eff}, P, N_{\rm H}, N_{\rm He}) = C_V - (N_{\rm H}+N_{\rm He})\frac{\beta_{\rm eff}}{\beta_{{\rm eff},\beta}}\frac{\hat{\eta}_{,\beta}}{\hat{\eta}}. \tag{5.21}$$

The thermal coefficient $\hat{\eta}$ defined in (5.7) is positive and its derivative $\hat{\eta}_{,\beta}$ in (5.20) negative, see the remarks after (5.27); the derivatives $\eta'_{\rm H,He}(\beta)$ needed to calculate $\hat{\eta}_{,\beta}$ are stated in (3.21). The inequalities $C_P > C_V > 0$ thus require $\beta_{\rm eff}(\beta, N_{\rm H}, N_{\rm He}) > 0$ and $\beta_{{\rm eff},\beta} > 0$ as necessary and sufficient conditions, cf. (5.10) and (5.16). The isobaric heat capacity C_P is calculated via (5.21) and recorded in Table 3.

The $\beta_{\rm eff}$ and P derivatives of the volume factor $V(\beta_{\rm eff}, P, N_{\rm H}, N_{\rm He})$ in (5.13),

$$V_{,\beta_{\rm eff}} = \frac{\hat{\eta}_{,\beta}}{\beta_{{\rm eff},\beta}}\frac{1}{P}, \quad V_{,P} = -\hat{\eta}\frac{1}{P^2}, \tag{5.22}$$

define the isothermal compressibility $\kappa_{T_{\rm eff}} = -V_{,P}/V = 1/P$, cf. Table 3, and the isobaric expansion coefficient,

$$\alpha_{\rm exp} = \frac{V_{,T_{\rm eff}}}{V} = -\beta_{\rm eff}^2\frac{V_{,\beta_{\rm eff}}}{V} = -\frac{\beta_{\rm eff}^2}{\beta_{{\rm eff},\beta}}\frac{\hat{\eta}_{,\beta}}{\hat{\eta}}, \tag{5.23}$$

which is positive if $\beta_{{\rm eff},\beta}(\beta, N_{\rm H}, N_{\rm He}) > 0$. The expansion coefficient is calculated via (5.23) and listed in Table 3. In equilibrium, $\hat{\eta} = (N_{\rm H}+N_{\rm He})/\beta$ and $\alpha_{\rm exp} = \beta_{\rm eff} = \beta$. The isobaric and isochoric heat capacities are related by the identity $C_P = C_V + (N_{\rm H}+N_{\rm He})\alpha_{\rm exp}/\beta_{\rm eff}$ (even though the gas mixture is not equilibrated), which provides a consistency check for the numerical estimates in Table 3.

5.6. Adiabatic compressibility of a gas mixture in stationary non-equilibrium

To obtain the $(S, P, N_{\rm H}, N_{\rm He})$ parametrization of the volume factor, we solve the entropy function $S(\beta, P, N_{\rm H}, N_{\rm He})$ in (5.17) for β,

$$\beta = \hat{g}^{-1}(S + (N_{\rm H}+N_{\rm He})(\log P - 1), N_{\rm H}, N_{\rm He}), \tag{5.24}$$

and substitute this into the thermal equation (5.7),

$$V(S, P, N_{\rm H}, N_{\rm He}) = \frac{1}{P}\hat{\eta}(\beta(S, P, N_{\rm H}, N_{\rm He}), N_{\rm H}, N_{\rm He}). \tag{5.25}$$

The pressure derivative thereof is

$$V_{,P} = \left(\frac{N_{\rm H}+N_{\rm He}}{\hat{g}_{,\beta}}\frac{\hat{\eta}_{,\beta}}{\hat{\eta}} - 1\right)\frac{\hat{\eta}}{P^2}, \tag{5.26}$$

with the derivatives $\hat{\eta}_{,\beta}$ and $\hat{g}_{,\beta}$ stated in (5.19) and (5.20). The adiabatic compressibility reads

$$\kappa_S = -\frac{V_{,P}}{V} = \frac{\kappa_{T_{\rm eff}}}{1+C_R}, \quad C_R(\beta, N_{\rm H}, N_{\rm He}) = \frac{N_{\rm H}+N_{\rm He}}{\beta_{\rm eff}\hat{u}_{,\beta}}\frac{\hat{\eta}_{,\beta}}{\hat{\eta}}, \tag{5.27}$$

with $\kappa_{T_{\rm eff}} = 1/P$, listed in Table 3 for cosmic-ray nuclei. Thus the identity $\kappa_{T_{\rm eff}}/\kappa_S = C_P/C_V$ obtained in Section 3.7 for a one-component gas also holds for a mixture in stationary non-equilibrium. Positivity of the coefficient C_R in (5.27) implies $0 < \kappa_S < \kappa_{T_{\rm eff}}$. C_R is positive, if $\beta_{\rm eff} > 0$, since $\hat{u}_{,\beta} < 0$, $\hat{\eta}_{,\beta} < 0$ and $\hat{\eta} > 0$. [$\hat{u}_{,\beta}$ is negative since it is a linear combination of $u'_{\rm H,He}(\beta)$ with positive coefficients, cf. (5.10), and $u'_{\rm H,He}(\beta) < 0$ is a Chebyshev inequality, see Section 3.8. The same holds true for $\hat{\eta}_{,\beta}$ in (5.20), with $\eta'_{\rm H,He}(\beta) < 0$ in (3.21). $\hat{\eta}$ in (5.7) is positive, since its coefficients $\eta_{\rm H,He}(\beta)$ are positive according to the integral representation in (3.6). The inequalities $0 < \kappa_S < \kappa_{T_{\rm eff}}$ and $C_P > C_V > 0$, cf. after (5.21), and the positivity of the expansion coefficient $\alpha_{\rm exp}$ in (5.23) are thus equivalent to a positive and monotonically increasing effective temperature, $\beta_{\rm eff} > 0$ and $\beta_{{\rm eff},\beta}(\beta, N_{\rm H}, N_{\rm He}) > 0$, where β is the decay exponent of the Weibull factor in flux density (4.1).

6. Conclusion

The measured all-particle cosmic-ray flux is highly isotropic and stationary, which suggests to treat the relativistic nuclei as a classical stationary non-equilibrium gas. Quantum effects and the Coulomb interaction can be discounted due to the low density and high temperature. The all-particle flux has been measured with good precision over an extended energy range, from 1 GeV up to 10^{11} GeV, so that even minor spectral breaks can be located in suitably rescaled flux maps, see Figs. 1 and 2. The multiply broken power-law distribution and the Weibull factor defining the spectral cutoff can be extracted from the flux data by way of a least-squares fit. The ultra-high energy spectral tail above 10^{10} GeV, measured with fluorescence and scintillation counters of the Telescope Array, exhibits subexponential decay and permits to infer the cutoff temperature and the decay exponent σ of the Weibull factor $\exp(-(E/(k_{\rm B}T))^{\sigma})$ quite accurately, cf. Table 2.

The multiply broken power-law distribution and the Weibull cutoff (setting in at about $k_{\rm B}T \approx 2.5\times 10^{10}$ GeV) determine the spectral number density of the nuclear gas. This density is the basis for the thermodynamic formalism developed here and can empirically be reconstructed from available flux data, cf. Fig. 3. This does not require to make specific assumptions about the driving forces generating the stationary non-equilibrium, the production, acceleration, scattering and absorption mechanisms cosmic-ray nuclei undergo, which are uncertain and would have to be specified in ab initio calculations based on kinetic equations. Currently contemplated production sites of cosmic-ray nuclei are Galactic supernova remnants and, in the case of ultra-high energy cosmic rays, active galactic nuclei [10]. The evidence for that is circumstantial, mainly from TeV gamma-ray spectra of a limited number of supernova remnants which can be explained by a radiation model involving high-energy protons. This model assumes gamma-ray emission by pion decay, the pions being produced in collisions of high-energy protons with heavier nuclei. High-energy protons can be produced by shock acceleration in supernova blast waves. The caveat here is that TeV gamma-rays can also be generated by inverse Compton scattering and tachyonic radiation processes [51], which do not require high-energy nuclei. The decay of the all-particle spectrum above 10^{10} GeV, cf. Fig. 2, could be caused by scattering of protons by cosmic microwave background photons, resulting in energy loss by pion production. Other attenuation mechanisms at high energy could be electron–positron pair production and photo-disintegration of heavy nuclei by interaction with the extragalactic background light. As it is presently not possible to quantify the production and absorption mechanisms, we have refrained from ab initio kinetic theory and extracted the number density of the nuclear gas from empirical spectra, cf. Section 4. To systematically model the fine structure of a multiply broken wideband spectrum requires a large number of parameters, as exemplified by the power-law function (4.4), which contains seven spectral breaks, cf. Table 1 and Figs. 1 and 2. Ab initio calculations of the all-particle wideband have not been attempted yet, although some of the mentioned acceleration and attenuation mechanisms have been tested in various energy ranges [10,52,53].

Apart from the specific example of cosmic-ray nuclei studied in Sections 4 and 5, we developed the thermodynamics of a classical stationary non-equilibrium gas (of relativistic particles) defined by a power-law distribution with Weibull spectral cutoff. In Section 2, we introduced the number density and the entropy functional, at first in spectral representation and then in relativistic phase space. The entropy functional substantially differs from an equilibrium entropy, as the multiply broken power law in the spectral number density generates excess entropy absent in an equilibrium system, and the Weibull entropy replaces the contribution of the internal energy to the entropy functional. In fact, Weibull entropy is quite unrelated to internal energy and only happens to coincide with U/T at spectral index $\sigma = 1$ where the Weibull exponential coincides with the Boltzmann factor, see (2.7). The spectral representation of the thermodynamic variables stated in Section 2 is suitable for numerical evaluation once the number density has been specified by a spectral fit; their phase-space representation is also derived in Section 2.

In Section 3, we invoked the entropy variable to define the effective temperature of a gas in stationary non-equilibrium and established the relation $\beta_{\rm eff}(\beta)$ between the effective gas temperature $\beta_{\rm eff} = 1/(k_{\rm B}T_{\rm eff})$ and the cutoff temperature $\beta = 1/(k_{\rm B}T)^{\sigma}$ in the Weibull exponential. We then derived the heat capacities and compressibilities of a stationary non-equilibrium gas and discussed thermodynamic inequalities such as $0 < C_V < C_P$, relating them to the positivity of the effective temperature parameter $\beta_{\rm eff}(\beta)$ and its derivative.

Cosmic-ray nuclei constitute a multi-component gas mixture because of the different particle masses. In Section 4, we represented the flux density of the all-particle spectrum as a two-component mixture composed of extended hydrogen and helium fluxes, $F_{\rm all} = F_{\rm H,ext} + F_{\rm He,ext}$, cf. Figs. 1 and 2. This reduction to a two-component system is possible as the low-energy spectrum consists almost exclusively of protons and helium nuclei and, above 10^4 GeV, the spectral density becomes ultra-relativistic so that the nuclear mass drops out and heavier nuclei can be accommodated in the hydrogen and helium flux components. In Section 5, we adapted the thermodynamic formalism developed in Section 3 to a two-component mixture and applied it to cosmic-ray nuclei. We extracted the partial number densities $\mathrm{d}\rho_{\rm H,ext}/\mathrm{d}p$ and $\mathrm{d}\rho_{\rm He,ext}/\mathrm{d}p$ of the nuclear gas (see Fig. 3) from the flux densities $F_{\rm H,ext}$, $F_{\rm He,ext}$ obtained from a least-squares fit to the all-particle spectrum, cf. Section 4 and Figs. 1 and 2. Finally we substituted the partial number densities into the spectral representations of the thermodynamic variables, cf. Section 2, to estimate the thermodynamic parameters of cosmic-ray nuclei: effective temperature, internal energy, pressure and entropy, as well as the heat capacities, the expansion coefficient and the isothermal and adiabatic compressibility of this non-equilibrated gas mixture, see Table 3.

References

[1] AMS Collaboration, Phys. Rev. Lett. 114 (2015) 171103.
[2] AMS Collaboration, Phys. Rev. Lett. 115 (2015) 211101.
[3] Y.S. Yoon, et al., Astrophys. J 728 (2011) 122.
[4] M. Amenomori, et al., Astrophys. J 678 (2008) 1165.
[5] IceCube Collaboration, Phys. Rev. D 88 (2013) 042004.
[6] IceCube Collaboration, Proc. Sci. (2015) PoS(ICRC2015)334.
[7] KASCADE-Grande Collaboration, Astropart. Phys. 36 (2012) 183.
[8] Pierre Auger Collaboration, Proc. Sci. (2015) PoS(ICRC2015)271.
[9] Telescope Array Collaboration, Proc. Sci. (2015) PoS(ICRC2015)035.
[10] A. Letessier-Selvon, T. Stanev, Rev. Modern Phys. 83 (2011) 907.
[11] I.A. Grenier, J.H. Black, A.W. Strong, Annu. Rev. Astron. Astrophys. 53 (2015) 199.
[12] W. Weibull, J Appl. Mech. 18 (1951) 293.
[13] NIST/SEMATECH e-Handbook of Statistical Methods, 2016. http://www.itl.nist.gov/div898/handbook//eda/section3/eda3668.htm.
[14] J.R. Šćepanović, et al., Physica A 392 (2013) 1153.
[15] J.C. Mauro, M.M. Smedskjaer, Physica A 391 (2012) 3446.
[16] D. Lynden-Bell, Physica A 263 (1999) 293.
[17] C.H. Lineweaver, C.A. Egan, Phys. Life Rev. 5 (2008) 225.
[18] R. Tomaschitz, Ann. Phys. 322 (2007) 667.
[19] R. Tomaschitz, Physica A 387 (2008) 3480.
[20] R. Tomaschitz, Physica A 394 (2014) 110.
[21] D. Cotto-Figueroa, et al., Icarus 277 (2016) 73.
[22] M. de Oliveira Santos, T. Stosic, B.D. Stosic, Physica A 391 (2012) 1546.
[23] R.D. Lorenz, et al., Planet. Space Sci. 70 (2012) 73.
[24] R.D. Lorenz, Icarus 264 (2016) 311.
[25] T. Hasumi, T. Akimoto, Y. Aizawa, Physica A 388 (2009) 491.
[26] T. Hasumi, T. Akimoto, Y. Aizawa, Physica A 388 (2009) 483.
[27] D.T. Hristopulos, V. Mouslopoulou, Physica A 392 (2013) 485.
[28] H. Fan, et al., Physica A 415 (2014) 172.
[29] S. Liang, et al., Physica A 452 (2016) 311.
[30] D.-X. Zhang, et al., Physica A 461 (2016) 299.
[31] J. Li, et al., Physica A 462 (2016) 508.
[32] I.L. Menezes-Sobrinho, A.L.S. Rodrigues, Physica A 389 (2010) 5581.
[33] J.C. Mauro, M.M. Smedskjaer, Physica A 391 (2012) 6121.
[34] G. Kaniadakis, M. Lissia, A.M. Scarfone, Phys. Rev. E 71 (2005) 046128.
[35] F. Clementi, et al., Physica A 387 (2008) 3201.
[36] D.T. Hristopulos, M.P. Petrakis, G. Kaniadakis, Entropy 17 (2015) 1103.
[37] D.T. Hristopulos, M.P. Petrakis, G. Kaniadakis, Phys. Rev. E 89 (2014) 052142.
[38] O.S. Garanina, M.Yu. Romanovsky, Physica A 427 (2015) 1.
[39] R. Tomaschitz, Astropart. Phys. 84 (2016) 36.
[40] R. Tomaschitz, Physica A 451 (2016) 456.
[41] R. Tomaschitz, Europhys. Lett. 106 (2014) 39001.
[42] R. Tomaschitz, Phys. Lett. A 378 (2014) 2337.
[43] R. Tomaschitz, Phys. Lett. A 378 (2014) 2915.
[44] R. Tomaschitz, Physica B 405 (2010) 1022.
[45] D. Band, et al., Astrophys. J. 413 (1993) 281.
[46] R.D. Preece, et al., Astrophys. J. Suppl. 126 (2000) 19.
[47] R. Tomaschitz, Physica A 385 (2007) 558.
[48] R. Tomaschitz, Phys. Lett. A 372 (2008) 4344.
[49] R. Tomaschitz, Phys. Lett. A 377 (2013) 3247.
[50] R. Tomaschitz, Europhys. Lett. 104 (2013) 19001.
[51] R. Tomaschitz, J. High Energy Astrophys. 8 (2015) 10.
[52] R. Aloisio, V. Berezinsky, A. Gazizov, Astropart. Phys. 39 (2012) 129.
[53] L. O'C. Drury, Astropart. Phys. 39 (2012) 52.